

26. SILICATE MINERALOGY OF BASALTS FROM THE EAST PACIFIC RISE, OCP RIDGE, AND SIQUEIROS FRACTURE ZONE: DEEP SEA DRILLING PROJECT LEG 54

R. N. Thompson and Susan E. Humphris,¹ Department of Geology, Imperial College of Science and Technology, London SW 7, England

ABSTRACT

Basalts drilled from the East Pacific Rise, OCP Ridge, and Siqueiros fracture zone during Leg 54 are texturally diverse. Dolerites are equigranular at Sites 422 and 428 and porphyritic, with phenocrysts of plagioclase (An_{69-73}) and Ca-rich clinopyroxene ($Ca_{42}Mg_{48}Fe_{10}$) at Site 427. The East Pacific Rise lavas and some of those from the OCP Ridge are fine-grained and porphyritic. The majority of the large crystals are clustered skeletal glomerocrysts of plagioclase (An_{64-77}), together with olivine (Fo_{80-87}), Ca-rich clinopyroxene, or both. Euhedral phenocrysts of plagioclase, together with olivine, Ca-rich clinopyroxene, and Cr-Al spinel in some cases, occur in most of the fine-grained lavas. These phenocrysts are small (maximum dimension <1 mm in all but one sample), sparse (combined modal amount <1% in all samples), and distinctive from the megacrysts which characterize many ocean-floor lavas.

In two East Pacific Rise lavas, zoned plagioclase (An_{83} cores) is the sole phenocryst phase. In other porphyritic lavas from all the main East Pacific Rise and OCP Ridge units drilled during Leg 54, the plagioclase phenocrysts contain cores of bytownite (An_{79-87}) surrounded by more-sodic feldspar (An_{67-77}). Core/rim relationships vary from continuous normal zoning, through discontinuous zoning, to extensive resorption of the calcic cores in some samples. The compositions of the plagioclase calcic cores are systematically related to those of the glomerophytic plagioclase and olivine in the lavas containing them. Furthermore, only one compositional population of calcic cores occurs in each rock. The possible causes of these relationships are far from clear. Magma mixing, although superficially applicable, is inconsistent with important aspects of the phenocryst mineralogy of these particular lavas. A more satisfactory model to explain both phenocryst zoning and rapid glomerocryst growth immediately before extrusion may be constructed by postulating influx of water into the upwelling magmas within Layer 3 of the oceanic crust beneath the East Pacific Rise, and subsequent loss of part of this water during effervescence within feeder dykes between Layer 3 and the ocean floor. It is shown that this model is fully consistent with published data on water and carbon dioxide contents and ratios in the pillow-margin glasses, vesicles, and phenocryst inclusions of ocean-floor basalts. The evidence for the precipitation of plagioclase-dominated crystalline assemblages from these magmas in the upper part of Layer 3 is concordant with recent geophysically based modeling of the structure of the East Pacific Rise.

Calcium-rich clinopyroxenes in dolerites from the OCP Ridge and Siqueiros fracture zone show radial, oscillatory, and sector-zoning. In Sample 428A-5-2 (Piece 5a), the compositional trends resulting from this zoning closely resemble those of the pyroxenes in some lunar lavas. The controls on crystallization of interstitial pigeonite—epitaxial upon augite—in this rock are discussed. Both sector-zoning of the augite and nucleation of pigeonite within microvolumes of magma with a low Ca(Mg + Fe) ratio appear to be important factors.

¹ Present address: (S. E. Humphris) Sea Education Association, Woods Hole, Massachusetts.

INTRODUCTION

Several of the sites drilled during DSDP Leg 54 yielded basalts which were produced along the East Pacific Rise spreading axis. This chapter contains a description of electron-probe microanalyses of the silicate minerals in nine samples, from all the main petrological units identified by the shipboard party at these locations (Sites 420, 421, 423, and 429). Also included are comparable data on seven representative samples from Sites 422 and 428, adjacent to the OCP Ridge, and two from Site 427, in the Siqueiros fracture zone (see Figure 1).

The present study has three main objectives. First, it contributes toward the detailed petrological description of the East Pacific Rise lavas, facilitating their comparison with those of other spreading axes. In this part of the work, we concentrate on determining the phenocryst mineralogy, and provide data for use in petrochemical calculations. Secondly, we compare phenocryst mineral compositions of basalts from the East Pacific Rise, OCP Ridge, and Siqueiros fracture zone. Thirdly, we investigate the complex zoning displayed by the pyroxenes in some of the coarse dolerites sampled during this Leg. We then compare these zoning trends with other terrestrial and lunar occurrences. They illuminate the general problem of how basalt magma crystallizes under various circumstances.

PETROGRAPHY

Humphris and Thompson (this volume) give a general account of the petrography of the Leg 54 basalts. Only the microprobe study is detailed here. In general, the basalts studied are moderately fractionated (Sites 422, 428, and part of 429) to highly fractionated ferrobasalts (Sites 421, 423, 427, and part of 429).

Megacrysts

The megacrysts of various minerals (5 mm or more in size), which are common in many ocean-floor basalts, are rare in this part of the East Pacific. The shipboard party noted a few, but none occurs within the 146 thin sections (two each from 73 specimens) in the collection used for this study. The phenocrysts in the Site 427 porphyritic dolerites are almost large enough (up to 2 mm in maximum dimension) to be called megacrysts, had they occurred in finer-grained rocks. As it is, they are only up to twice as large as the coarse groundmasses of the dolerites containing them.

Phenocrysts: A Problem of Definitions

The samples used for microprobe studies include four OCP Ridge equigranular dolerites [Samples 422-7-1 (Piece 9), 422-8-5 (Piece 14), 428A-5-2 (Piece 5a), and 428A-6-1 (Piece 6)] and two Siqueiros fracture zone porphyritic dolerites [Samples 427-10-3 (Piece 3) and 427-11-1 (Piece 3)]. The remaining 12 lavas are all extremely fine grained, and contain varying amounts of microphe- nocrysts with diverse morphologies (Plate 1, Figures 1 through 8), as follows:

1) Some samples have clear-cut porphyritic textures, containing euhedral microphe- nocrysts, 0.2 to 1.5 mm in

size, set in groundmasses of either spherulitically devit- rified glass or microgranular silicate crystals. Examples of this group are Samples 421-3-1 (Piece 14) (plagioclase and olivine-phyric; Plate 1, Figure 2), 423-8-1 (Piece 4) (plagioclase and augite-phyric; Plate 1, Figure 3), and Samples 421-3-1 (Piece 8) and 429A-2-1 (Piece 16) (plagioclase-phyric). The plagioclase microphe- nocrysts are sub-equant, with elongations not exceeding 5:1.

2) Other samples are typical representatives of the glomerophytic texture which is widespread in ocean- floor basalts. These contain stellate clusters of plagioclase, together with olivine [Samples 429A-2-1 (Piece 4a); Plate 1, Figure 3; 428-5-4 (Piece 2); Plate 1, Figure 5; 428-6-2 (Piece 12); Plate 1, Figure 4], augite [Samples 420-13,CC (Piece 1); Plate 1, Figure 6, 423-7-1 (Piece 6), 423-8-1 (Piece 4)] or both [Samples 420-16-1 (Piece 1), 421-4-1 (Piece 3), and 422-9-2 (Piece 4c); Plate 1, Figure 7]. In specimens such as Samples 420-16-1 (Piece 1) and 429A-2-1 (Piece 4a) (Plate 1, Figure 3), from the chilled margins of pillow lavas, the glomerophytic clusters are evenly distributed in a matrix of fresh glass. Microprobe analyses of such glasses in dredge hauls and DSDP drill cores (e.g., Byerly et al. 1977; Thompson, in press) show that they are extremely homogenous in chemical composition throughout eruptive units, implying that any crystals within them grew entirely before extrusion of the magma. In contrast, specimens such as Sample 420-13,CC (Piece 1) (Plate 1, Figure 6) contain glomerophytic clusters that vary widely in the size of their constituent crystals and distribution. Thus, areas of a thin section up to 3 × 1 mm are almost totally devoid of crystals exceeding 0.05 mm, while adjacent areas are full of plagioclase laths up to 0.8 mm in length. Such a texture seems to imply differential movement of liquid and glomerophytic clusters, together with some post- extrusion growth of the latter. In view of the diverse textures shown by the glomerocrysts in Leg 54 samples, we describe them separately from the equant, non-skeletal, isolated phenocrysts throughout this chapter.

3) Hybrids between the two previous textural types are provided by specimens which contain sub-equant, euhedral, isolated phenocrysts of various phases, in addition to glomerophytic clusters. In specimens such as Samples 421-3-1 (Piece 14) (Plate 1, Figure 2) and 423-8-1 (Piece 4) (Plate 1, Figure 1), the relationship is un- ambiguous, because the true phenocrysts are larger than their glomerophytic neighbors. As the latter become coarser, the distinction between phenocrysts and glomerocrysts is progressively more difficult to make. In extreme cases, such as Samples 420-13,CC (Piece 1) (Plate 1, Figure 6) and 422-9-2 (Piece 4c), (Plate 1, Figure 7), the skeletal plagioclase glomerocrysts are longer than the phenocrysts associated with them, and the latter may be detected only by means of their morphology and compositions.

The concept that the first-formed plagioclases in some of the Leg 54 lavas have smaller maximum dimen- sions than their associated "groundmass" plagioclases produces a nomenclature problem. In this account these first-formed crystals are called "phenocrysts," obvi- ating the use of any term that is more precise but also

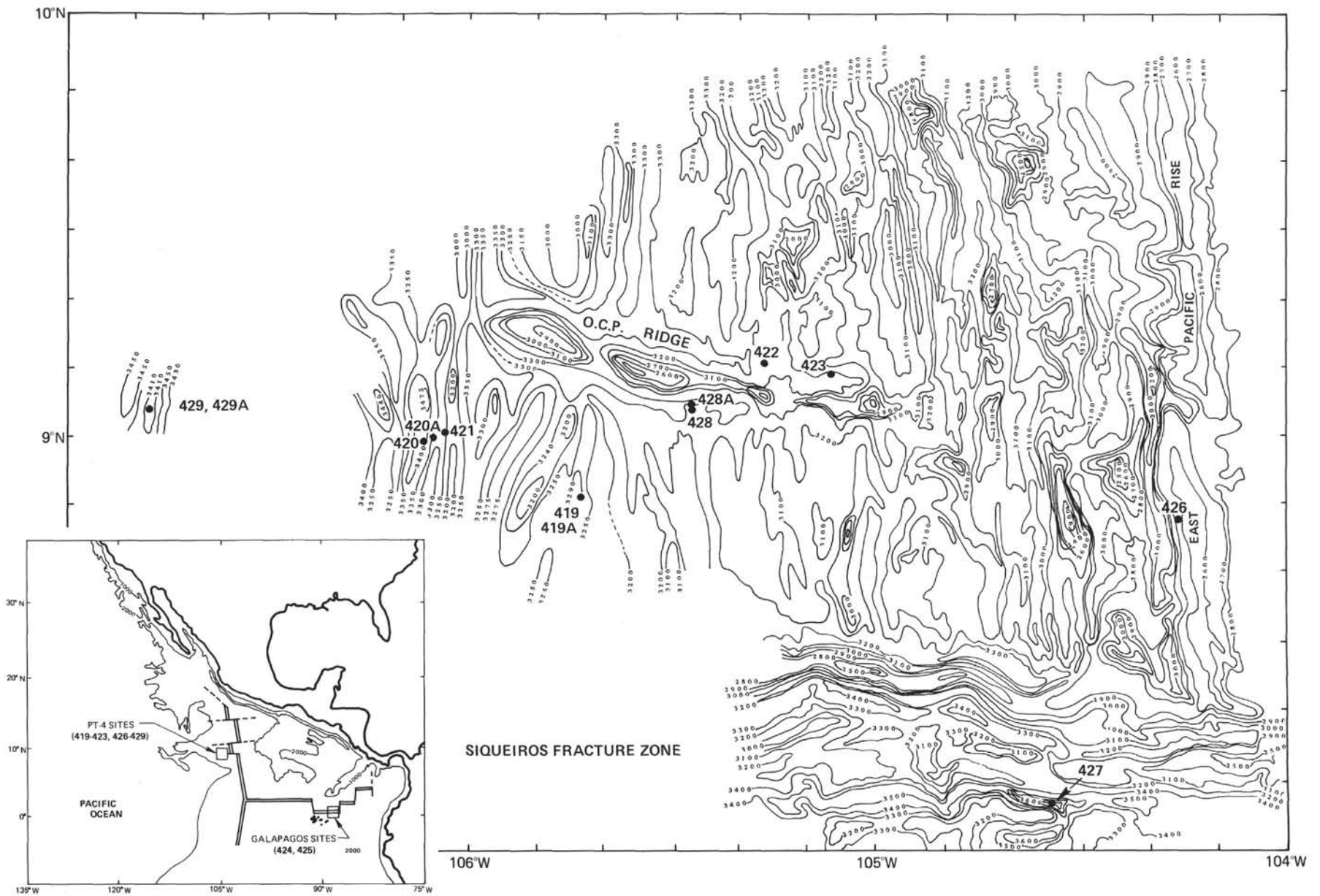


Figure 1. The East Pacific Rise near the Siqueiros fracture zone, showing Leg 54 drill sites. Contours in corrected meters.

more cumbersome. It may well be that these sub-equant, euhedral crystals contain more plagioclase by volume than the long but thin and skeletal glomerocrysts accompanying them.

PHENOCRYSTS

Modes and Sizes

Modal analyses of the samples used for mineralogical study are given in Table 1. The spacing of the point-counting grid was 0.15×0.2 mm. The number of points varied from 2000 to 5000, depending on the grain size and texture of each rock. There are two main sources of error in these modes. First, in all samples that do not have a glassy groundmass a problem of varying severity exists as to which points falling on very small crystals should be allocated to fine-grained glomerophyritic clusters and which points to call groundmass. Secondly, the abundances of non-glomerophyritic, non-skeletal phenocrysts are so low in all the samples that they are too sparsely distributed to be sampled adequately by a single thin section.

The maximum dimensions of the various crystal groups recorded in the modal analyses are also listed in Table 1. Apart from the Site 427 porphyritic dolerites and Site 422 and 428 equigranular dolerites, the samples used in this study are very fine grained. Their phenocryst contents involve problems of definition, as discussed above. Some of the samples are virtually aphyric, by any definition. Others contain up to 20 volume per cent of phenocrysts. Nevertheless, the amounts of equant or sub-equant, euhedral, isolated phenocrysts in all the fine-grained lavas do not exceed 0.5 per cent, so that the large majority of the phenocrysts in the more porphyritic samples are elongate, skeletal crystals in glomerophyritic groups. This point needs to be emphasized, because it affects any discussion of crystal fractionation or accumulation in the Leg 54 lavas. The non-skeletal phenocrysts are suitable for consideration in terms of Stokes' Law. In contrast, the stellate glomerophyritic clusters of diverse skeletal crystals must float or sink far less readily in basic magma than spheres of equivalent volume.

The skeletal crystal morphologies imply rapid growth rates. Specifically, the olivines in Samples 420-16-1 (Piece 1) and 429A-2-1 (Piece 4a) (Plate 1, Figure 3) are excellent examples of hopper olivines, in the terminology of Donaldson (1976). The experiments at 1 atmosphere by Donaldson (1976) on ocean-floor basalts demonstrate that hopper olivines probably grow in these normative-olivine-poor melts under conditions of considerable undercooling. Similarly, the experiments of Lofgren and Donaldson (1975) indicate that appreciable supercooling is a prerequisite for the growth of elongate, curved, skeletal plagioclases, as are characteristic of the Leg 54 glomerocrysts.

Compositions

The electron probe microanalyses were made at Imperial College, using a Cambridge Instruments Microscan \bar{V} probe fitted with a Link EDS detector. The operating conditions were as follows: accelerating voltage = 15 kv, specimen current = $0.01 \mu\text{a}$, counting time = 100 s for all phases except feldspar (50 s), beam focused to its minimum spot.

Table 2 summarizes the core compositions of phenocrysts (including glomerocrysts) in the 14 porphyritic samples from Leg 54 used in this study. In addition, the most calcic plagioclases and ferromagnesian mineral analyses with the highest Mg/Fe ratio in four equigranular OCP Ridge dolerites are also listed. The following convention is used in this table. If all the analyses of the cores of a phenocryst mineral in a given rock vary by less than 3 per cent in major components (such as mole per cent forsterite or anorthite), that phase is recorded as unzoned and the mean composition is given. For minerals with greater core-composition ranges, the most Mg-rich olivine and pyroxene and Ca-rich plagioclase are recorded. Representatives of the 510 mineral analyses obtained during this study are given in Table 3. When using the data in this table, it should be remembered that EDS microprobes are less sensitive to small amounts of elements than wavelength-dispersive systems. Values of oxides below 0.2 per cent for light elements, such as

TABLE 1
Lava Phenocryst Modes and Sizes, Leg 54

Sample	Olivine Phenocrysts	Olivine Glomerocrysts	Plagioclase Phenocrysts	Plagioclase Glomerocrysts	Pyroxene Phenocrysts	Pyroxene Glomerocrysts	Spinel Phenocrysts	Groundmass	Vesicles
420-13, CC-1	—	—	0.1(0.3)	7.1(0.8)	0.4(0.4)	9.2(0.3)	—	78.3	4.9
420-16-1 (Piece 1)	—	0.2(0.5)	Tr ^a (0.3)	1.1(0.8)	0.2(0.3)	0.4(0.2)	—	97.3	0.8
421-3-1 (Piece 8)	—	—	0.1(0.3)	—	—	—	—	99.6	0.3
421-3-1 (Piece 14)	0.1(0.3)	—	0.2(0.5)	—	—	—	—	99.1	0.6
421-4-1 (Piece 3)	—	Tr(0.2)	0.2(0.7)	2.6(0.6)	—	3.2(0.2)	—	93.1	0.9
423-7-1 (Piece 6)	—	—	0.1(0.4)	0.9(0.5)	—	0.8(0.1)	—	97.9	0.3
423-8-1 (Piece 4)	—	—	0.4(1.5)	0.8(0.4)	Tr(0.2)	1.5(0.1)	—	97.2	0.1
429A-2-1 (Piece 4a)	—	1.0(0.5)	—	5.5(0.9)	—	—	—	92.6	0.9
429A-2-1 (Piece 16)	—	—	0.2(0.4)	—	—	—	—	98.9	0.9
422-9-2 (Piece 4c)	—	1.4(0.2)	0.4(0.5)	16.5(0.9)	—	2.0(Arb)	Tr(0.04)	79.3	0.4
428-5-4 (Piece 2)	—	2.0(0.2)	—	4.9(0.8)	—	—	—	91.5	1.6
428-6-2 (Piece 12)	—	0.3(0.1)	—	1.9(0.9)	—	—	—	97.3	0.5
427-10-3 (Piece 3)	—	—	2.6(1.7)	—	1.6(0.9)	—	—	95.8	Dolerite
427-11-1 (Piece 3)	—	—	1.2(2.0)	—	0.2(0.6)	—	—	98.6	Dolerite

Note: Modal amounts are in volume per cent. The figure in parentheses beside each modal amount is the maximum dimension of that phase in mm. Arb = arborescent.
^aTr = less than 0.1 vol. %.

TABLE 2
Compositions of Phenocryst Cores and Centers of Zoned Crystals in Dolerites, Leg 54

East Pacific Rise Sites									
Sample	420-13, CC (Piece 1)	420-16-1 (Piece 1)	421-3-1 (Piece 8)	421-3-1 (Piece 14)	421-4-1 (Piece 3)	423-7-1 (Piece 6)	423-8-1 (Piece 4)	429A-2-1 (Piece 4a)	429A-2-1 (Piece 16)
Texture	Porphyritic	Porph	Porph	Porph	Porph	Porph	Porph	Porph	Porph
Olivine (Fo)	—	80 U	—	80 U	78 U	—	—	87 U	—
Plagioclase (An)	67 Z (70-79)	70 Z	83 Z	71 U (79)	69 U	71 U	72 U	76 U	82 Z
Pyroxene	Ca	41 U	41 U	—	—	42-30 S	38-27 S	42-37 S	—
	Mg	49	49	—	—	43-56	49-58	48-50	—
	Fe	10	10	—	—	15-14	13-15	10-13	—
OCP Ridge and Siqueiros Fracture Zone Sites									
Sample	422-7-1 (Piece 9)	422-8-5 (Piece 14)	422-9-2 (Piece 4c)	428-5-4 (Piece 2)	428-6-2 (Piece 12)	428A-5-2 (Piece 5a)	428A-6-1 (Piece 6)	427-10-3 (Piece 3)	427-11-1 (Piece 3)
Texture	Doleritic	Dol	Porph	Porph	Porph	Dol	Dol	Porph	Porph
Olivine (Fo)	85 U	85 U	87 U	85 U	86 U	—	84 U	—	—
Plagioclase (An)	69 Z	79 Z	77 Z (87)	75 Z (85)	76 Z	70 Z	74 Z	69 U	73 U
Pyroxene	Ca	43-31 S	43-34 S	Cr-Al	—	—	41 U	45-39 S	41 U
	Mg	46-56	48-55	Spinel	—	—	50	47-52	48
	Fe	11-13	9-11	—	—	—	9	8-9	11

Note: U = unzoned; Z = radial-zoned; S = sector-zoned. See text for discussion of these terms. The bracketed plagioclase compositions are calcic cores within phenocrysts.

Na and Mg, and below 0.1 per cent for heavier elements, such as Fe, are probably not reliable.

Olivine

No significant zoning was detected in any of the olivines in Leg 54 samples. Only the solitary, equant, euhedral 0.3-mm crystal in Sample 421-3-1 (Piece 14) may reasonably be described as a phenocryst. In all the other olivine-bearing porphyritic samples this phase either adopts strongly skeletal morphologies or occurs as tiny equant grains, up to 0.2 mm in size, in glomerophytic groups. Microprobe analyses of the fresh basaltic glass in chilled parts of the olivine-bearing Samples 420-16-1 (Piece 1) and 429A-2-1 (Piece 4a) are reported by Humphris and Thompson (accompanying chapter). If Fe_2O_3 in the glass is taken to be 1.1 per cent—i.e., the value in the Smithsonian Institution MORB glass standard USNM 113716 (Thompson, in press)—the ratio of Fe/Mg in olivine to Fe^{+2}/Mg in surrounding glass is 0.27 for Sample 420-16-1 (Piece 1) and 0.26 for Sample 429A-2-1 (Piece 4a). These values are a little lower than those obtained in equilibrium experiments (Roeder and Emslie, 1970; Thompson, 1974), but they are close to the coefficients obtained in other studies of olivine compositions in ocean-floor lavas (Donaldson, 1975a; Hekimian et al., 1976).

Plagioclase

The porphyritic, fine-grained samples from both the East Pacific Rise and OCP Ridge suites show similar complexities of plagioclase morphology and composition; they are therefore treated together. As already described, plagioclase occurs in two forms within these porphyritic rocks: as sub-equant isolated euhedra, and

as glomerophytic elongate skeletal crystals which are often curved. These types coexist in varying proportions and have textures that depend upon the relative sizes of the two crystal forms.

The glomerophytic/elongate plagioclases have cores which are unzoned in some samples and normally zoned in others. The range of glomerophytic plagioclase core compositions found in the Leg 54 lavas examined during this study is An_{64} to An_{77} . The normal zoning in their rims amounts to only a few per cent An, in contrast with coarsely doleritic samples, such as Sample 428A-5-2 (Piece 5a), where the zoning extends to An_{16} .

The euhedral, isolated plagioclase phenocrysts are unzoned—with or without faint oscillations—in some samples and zoned in others. Two of the East Pacific Rise specimens, Samples 421-3-1 (Piece 8) and 429A-2-1 (Piece 16), contain phenocrysts of plagioclase alone. In both cases these are zoned, with An_{82} -to- An_{83} cores and An_{59} -to- An_{72} rims. Three other East Pacific Rise lavas [Samples 421-3-1 (Piece 14) (Plate 1, Figure 2), 423-7-1 (Piece 6), and 423-8-1 (Piece 4) (Plate 1, Figure 1)], contain euhedral phenocrysts of plagioclase and olivine or clinopyroxene. This plagioclase is homogeneous An_{71} to An_{72} , except for a narrow zoned rim. In Sample 421-3-1 (Piece 14) there are a few small rounded areas of An_{79} composition within the An_{71} phenocrysts. OCP Ridge Sample 422-9-2 (Piece 4c) contains abundant elongate plagioclase glomerocrysts with An_{77} core compositions (Plate 1, Figure 7). Within the largest of these are sub-equant inner cores of An_{87} , which are unzoned except for faint oscillations and have sharp euhedral margins. The other two OCP Ridge lavas studied, Samples 428-5-4 (Piece 2) (Plate 1, Figure 5) and 428-6-2 (Piece 12), contain zoned glomerophytic plagioclase with

TABLE 3
Representative Microprobe Analyses of Minerals in Leg 54 Basalt and Dolerite Samples

Sample Analysis No. Mineral	420-13, CC (Piece 1)				420-16-1 (Piece 1)			421-3-1 (Piece 8)		421-3-1 (Piece 14)					421-4-1 (Piece 3)			
	1/1 Plag	1/2 Plag	1/3 Aug	1/4 Aug	2/1 Ol	2/2 Plag	2/3 Aug	3/1 Plag	3/2 Plag	4/1 Ol	4/2 Plag	4/3 Plag	4/4 Plag	4/5 Aug	4/6 Aug	5/1 Ol	5/2 Plag	5/3 Aug
SiO ₂	50.41	51.93	51.96	49.35	38.93	51.20	52.13	48.49	52.06	38.45	49.73	51.82	53.78	49.75	50.90	38.58	51.75	51.50
Al ₂ O ₃	31.32	29.36	2.67	5.01	—	29.75	2.80	32.24	30.21	—	31.44	30.55	28.35	4.77	2.86	—	29.93	3.09
Cr ₂ O ₃	— ^b	—	0.57	0.20	—	—	0.88	—	—	—	—	—	—	—	—	—	—	0.47
FeO ^a	0.48	0.56	6.18	8.21	18.63	0.57	6.00	0.66	0.52	18.93	0.56	0.43	0.69	10.08	15.03	20.61	0.67	7.92
MnO	—	—	0.23	—	0.19	—	0.16	—	—	0.20	—	—	—	0.29	0.32	0.30	—	0.21
MgO	0.26	0.26	16.79	15.80	42.11	0.28	17.07	0.36	—	41.59	0.25	—	0.23	15.78	16.12	40.60	—	17.03
NiO	—	—	—	—	—	—	—	—	—	—	—	—	—	—	—	—	—	—
CaO	15.66	14.14	20.50	19.24	0.27	14.50	20.05	16.54	14.44	0.29	15.24	14.16	12.82	17.73	13.08	0.31	14.36	18.55
Na ₂ O	2.28	3.82	—	0.29	—	3.41	0.27	1.93	3.11	—	2.30	3.16	4.20	—	0.54	—	3.52	0.31
K ₂ O	—	—	—	—	—	—	—	—	—	—	—	—	—	—	—	—	—	—
TiO ₂	—	—	0.50	1.38	—	—	0.50	—	—	—	—	—	—	1.35	0.90	—	—	0.83
Total Cation Proportions No. of oxygens	100.41	100.07	99.40	99.48	100.13	99.71	99.86	100.22	100.34	99.46	99.52	100.12	100.07	99.57	99.75	100.40	100.23	99.91
Si	9.166	9.470	1.919	1.836	0.993	9.376	1.914	8.883	9.441	0.990	9.122	9.409	9.755	1.849	1.911	0.991	9.421	1.899
Al	6.715	6.312	0.117	0.220	—	6.423	0.122	6.963	6.459	—	6.799	6.539	6.062	0.210	0.127	—	6.423	0.135
Cr	—	—	0.017	0.006	—	—	0.026	—	—	—	—	—	—	—	—	—	—	0.014
Fe	0.072	0.086	0.190	0.255	0.396	0.086	0.184	0.102	0.078	0.406	0.085	0.064	0.105	0.313	0.470	0.441	0.102	0.244
Mn	—	—	0.007	—	0.005	—	0.006	—	—	0.005	—	—	—	0.009	0.011	0.007	—	0.007
Mg	0.071	0.069	0.924	0.876	1.600	0.077	0.934	0.099	—	1.595	0.068	—	0.062	0.877	0.902	1.554	—	0.936
Ni	—	—	—	—	—	—	—	—	—	—	—	—	—	—	—	—	—	—
Ca	3.050	2.763	0.812	0.767	0.007	2.845	0.789	3.247	2.807	0.008	2.995	2.755	2.492	0.709	0.527	0.009	2.801	0.733
Na	0.805	1.350	—	0.021	—	1.212	0.020	0.685	1.093	—	0.817	1.111	1.478	—	0.040	—	1.243	0.023
K	—	—	—	—	—	—	—	—	—	—	—	—	—	—	—	—	—	—
Ti	—	—	0.014	0.039	—	—	0.014	—	—	—	—	—	—	0.038	0.026	—	—	0.024
Σ	19.879	20.050	4.000	4.020	3.001	20.019	4.009	19.979	19.878	3.004	19.886	19.878	19.954	4.005	4.014	3.002	19.990	4.015

An₇₅-to-An₇₆ cores. One such crystal in Sample 428-5-4 (Piece 2) encloses a small, oval, unzoned An₈₅ inner core.

To summarize, cores of calcic bytownite composition (An₈₂₋₈₇) are widespread within the plagioclase phenocrysts of both East Pacific Rise and OCP Ridge lavas drilled during Leg 54. In some East Pacific Rise samples these calcic cores are zoned continuously outward to the compositions of the glomerophytic plagioclases containing them. But in most Leg 54 samples, there is a clear compositional gap of 8 to 10 per cent anorthite component (with or without resorption), followed by the precipitation of more-sodic plagioclase mantles and rims to the phenocrysts.

Another empirical mineralogical relationship in the Leg 54 samples concerns the compositions of coexisting olivine and plagioclase. In all six samples containing these phases within glomerophytic clusters, the forsterite content of the olivine is 10 (±1) per cent greater than the anorthite content of the associated plagioclase.

Cr-Al Spinel

Spinel occurs as a phenocryst in only one of the Leg 54 rocks studied in detail. It form tiny, very sparse euhedra in Sample 422-9-2 (Piece 4c), from the OCP Ridge. These crystals are located only within, or partially within, the calcic bytownite cores contained in a small proportion of the plagioclase glomerocrysts in this lava (see above). In contrast, the olivine microphenocrysts in Sample 422-9-2 (Piece 4c) are only found intergrown with the sodic bytownite outer parts of the plagioclases. It therefore appears from the texture that olivine and Cr-Al spinel did not coprecipitate in this rock. The ratio of Al₂O₃ in Sample 422-9-2 (Piece 4c) to that in its spinel microphenocrysts is the same as reported for Leg 37 basalt spinels by Sigurdsson (1977) (his Figure 5).

Clinopyroxene

The only phenocryst pyroxene in Leg 54 samples is Ca-rich clinopyroxene, within the compositional range

of endiopside-augite (approaching sub-calcic augite). There are difficulties in interpreting the textures and zoning of this pyroxene. In specimens with simple porphyritic textures, such as Samples 423-8-1 (Piece 4), 427-10-3 (Piece 3), and 427-11-1 (Piece 3), the pyroxene forms euhedral or subhedral, equant phenocrysts. These coexist with phenocrysts of plagioclase alone, except for a trace of olivine in Sample 420-16-1 (Piece 1).

Clinopyroxene is also a component of the glomerophytic clusters in many Leg 54 samples. As with plagioclase, the status of the pyroxene glomerocrysts varies from groundmass, in tiny stellate clusters around phenocrysts, to that of a component of relatively coarse glomerophytic clusters, where it can be argued that this phase is a phenocryst. The glomerophytic pyroxenes are characterized by shadowy extinction and irregular sector-zoning. The latter is easy to observe optically when the crystals are subhedral, but is revealed only by microprobe analyses in cases where the crystals are skeletal.

The composition of the pyroxene in unequivocal phenocrysts does not differ significantly from Ca₄₁Mg₄₉Fe₁₀, in all the rocks where this phase occurs (Tables 1 and 2). The glomerophytic pyroxenes are all slightly more Fe-rich than this. They show two types of zoning: varying Mg/Fe ratio at approximately constant Ca/(Mg+Fe) ratio and varying Ca/(Mg+Fe) ratio at approximately constant Mg/Fe ratio. In skeletal crystals, the latter type resembles the "quench trend" described by Smith and Lindsley (1971). Nevertheless, in samples with subhedral glomerophytic pyroxenes, it is clear from both the optics of the crystals and the bimodality of the microprobe analyses that this sub-calcic "trend" is in fact the result of sector- rather than radial-zoning. Bence et al. (1975) reached a similar conclusion in their discussion of Late Cretaceous ocean-floor basalts drilled in the central Caribbean during DSDP Leg 15. The sector-zoned pyroxenes are listed as such in Table 2.

The minor elements in the pyroxenes of the Leg 54 samples are useful indicators of various aspects of their crystallization. Chromium shows strong radial deple-

TABLE 3 – Continued

423-7-1 (Piece 6)				423-8-1 (Piece 4)		429A-2-1 (Piece 4a)		429A-2-1 (Piece 16)		422-7-1 (Piece 9)					422-8-5 (Piece 14)		
6/1 Plag	6/2 Plag	6/3 Aug	6/4 Aug	7/1 Plag	7/2 Aug	8/1 Ol	8/2 Plag	9/1 Plag	9/2 Plag	10/1 Ol	10/2 Plag	10/3 Aug	10/4 Aug	10/5 Aug	11/1 Ol	11/2 Plag	11/3 Aug
51.59	52.74	51.51	54.52	51.47	52.54	40.46	50.74	49.32	54.23	40.13	52.06	51.36	54.11	49.86	40.77	50.29	52.12
30.00	28.62	3.60	1.44	30.11	2.19	—	30.04	30.68	28.20	—	29.60	3.85	1.51	2.27	—	30.83	3.38
—	—	0.54	0.24	—	0.49	—	—	—	—	—	—	0.29	0.31	—	—	—	0.35
0.47	0.68	7.26	9.22	0.40	6.31	12.18	0.60	0.56	0.64	14.57	0.58	6.50	7.01	17.38	14.74	0.35	5.37
—	—	0.17	0.29	—	0.22	0.19	—	—	—	0.21	—	0.17	0.21	0.40	0.16	—	0.19
—	0.28	16.05	20.78	0.16	16.48	46.84	0.28	0.39	0.40	44.76	0.24	16.28	19.98	11.71	44.89	0.22	16.80
—	—	—	—	—	—	—	—	—	—	—	—	—	—	—	—	—	—
14.54	13.18	19.08	13.43	14.60	20.50	0.26	15.21	16.17	12.29	0.26	14.26	19.90	15.84	16.58	0.29	15.91	20.93
3.26	4.01	0.32	—	3.08	—	—	2.58	2.15	4.64	—	3.48	—	—	—	—	2.33	0.39
—	—	0.78	0.47	—	0.50	—	—	—	—	—	—	0.72	0.31	1.53	—	—	0.58
99.86	99.51	99.31	100.39	99.82	99.23	99.93	99.45	99.27	100.40	9.93	100.22	99.07	99.28	99.73	100.85	99.93	100.11
32	32	6	6	32	6	4	32	32	32	4	32	6	6	6	4	32	6
9.414	9.639	1.906	1.971	9.392	1.942	1.002	9.314	9.105	9.797	1.005	9.468	1.900	1.973	1.913	1.010	9.195	1.906
6.454	6.166	0.158	0.062	6.476	0.096	—	6.501	6.677	6.006	—	6.346	0.168	0.065	0.103	—	6.645	0.146
—	—	0.016	0.007	—	0.015	—	—	—	—	—	—	0.009	0.009	—	—	—	0.011
0.071	0.104	0.224	0.278	0.061	0.194	0.252	0.092	0.086	0.097	0.304	0.087	0.201	0.213	0.555	0.304	0.054	0.164
—	—	0.016	0.009	—	0.007	0.005	—	—	—	0.005	—	0.006	0.006	0.014	0.004	—	0.006
—	0.077	0.885	1.120	0.045	0.908	1.729	0.076	0.107	0.108	1.670	0.065	0.898	1.086	0.670	1.657	0.060	0.916
—	—	—	—	—	—	—	—	—	—	—	—	—	—	—	—	—	—
2.842	2.581	0.757	0.520	2.855	0.812	0.007	2.992	3.198	2.380	0.007	2.779	0.789	0.619	0.682	0.008	3.117	0.820
1.154	1.423	0.023	—	1.088	—	—	0.920	0.771	1.625	—	1.227	—	—	—	—	0.827	0.028
—	—	0.022	0.013	—	0.015	—	—	—	—	—	—	0.021	0.008	0.045	—	—	0.016
19.935	19.990	4.007	3.980	19.917	3.989	2.995	19.895	19.944	20.013	2.991	19.972	3.992	3.979	3.982	2.983	19.898	4.013

tion from cores to rims of crystals, even in phenocrysts which are otherwise unzoned. Sodium concentrations are below the detection limit of the EDS microprobe (~0.2 per cent Na₂O) in many analyses. Consideration of the cation charge balance suggests that most of these pyroxenes contain little Fe³⁺.

The Al and Ti contents of phenocrysts and glomerocrysts in the Leg 54 samples are useful for distinguishing these two types of pyroxene occurrence. Figure 2 shows the Si and Al cation proportions (0 = 6) of all the pyroxenes analyzed during this study. The isolated pyroxene phenocrysts in East Pacific Rise and Siqueiros fracture zone samples and the cores of large pyroxene grains in OCP Ridge dolerites all exhibit similar large ranges of Si and Al on Figure 2. All these pyroxenes contain both tetrahedrally and octahedrally coordinated Al. Below a cation proportion of Al = 0.1, the amount of Al^{IV} varies, whereas Al^{VI} remains approximately constant. Above Al = 0.1 on Figure 2, there is an increase in Al^{VI} as Al^{IV} rises. The pyroxenes in glomerophytic clusters (both coarse and fine-grained) show a distinctive trend on Figure 2. They range to lower values of Si and higher Al than the isolated phenocrysts, but, at an equivalent Si value, they contain less Al^{VI} than the latter. It is important to note that the pyroxene glomerocryst data include analyses of crystals in Sample 421-3-1 (Piece 14), where this phase is definitely in the groundmass (Plate 1, Figure 2). It should therefore be stressed that the minor-element chemistry of the glomerocrysts, even when they are in relatively coarse clusters, is distinct from that of unequivocal pyroxene phenocrysts in these rocks, and continuous with that of the skeletal groundmass pyroxenes in the porphyritic lavas.

Figure 3 is a plot of Ti and Al in clinopyroxene phenocrysts, glomerocrysts, and the centers of coarse crystals in dolerites. Data for pyroxenes in the three dolerites [Samples 422-7-1 (Piece 9), 428A-5-2 (Piece 5a), and 427-10-3 (Piece 3)] subjected to detailed study are not included in this diagram (see Figures 4 and 5). The isolated phenocrysts and dolerite crystal-core analyses fall

along a narrow trend on Figure 3. There is a marked lack of points with values of Al between 0.095 and 0.115; the trend also shows a kink at this point. It is clear from the data on individual crystals that these features of Figure 3 are due to sector-zoning in the Leg 54 pyroxenes.

It has not been possible to assign crystallographic indices to these irregularly developed sector-zones in very small pyroxene microphenocrysts. This matter will be considered further in discussing the coarse OCP Ridge dolerite Sample 428A-5-2 (Piece 5a). If the data of Figures 2 and 3 are combined, it is apparent that the Ti-poor zone (or zones) is also relatively depleted in Al^{IV} and Al^{VI}, while the Ti-rich zone (or zones) is richer in Al with both coordinations. It is also clear from Table 3 that most of the Al^{VI} is accommodated in these pyroxenes in the form of Ca-Tschermak's component, CaAl₂SiO₆.

The analyses of glomerophytic pyroxenes plotted on Figure 3 have high values of Ti and Al, which overlap and extend the range established by the phenocrysts. Moreover, the relative enrichment of the glomerocrysts in Ca-Tschermak's component is striking. In the Leg 54 lavas this pyroxene is located in the groundmass (in some samples) of tholeiitic lavas, where CATS substitution should be minimized during equilibrium crystallization. It seems probable that the anomalous chemistry of the glomerophytic pyroxenes is due to their rapid metastable growth under supersaturated conditions. This view is consistent with the forementioned observations on the crystal morphology of plagioclase and olivine in the glomerophytic lavas and with the occurrence of skeletal clinopyroxene in some samples [e.g., Sample 422-9-2 (Piece 4c)].

Influence of Water on Phenocryst Compositions

Table 4 gives the order of crystallization in the 14 porphyritic samples used in this study, as deduced from their textures and mineral compositions. The crystallization sequences of the Siqueiros fracture zone samples from Site 427 appear to be simple, comprising liquidus

TABLE 3 — Continued

Sample Analysis No. Mineral	422-9-2 (Piece 4c)				428-5-4 (Piece 2)			428-6-2 (Piece 12)		428A-5-2 (Piece 5a)									
	12/1 Ol	12/2 Plag	12/3 Plag	12/4 Spin	13/1 Ol	13/2 Plag	13/3 Plag	14/1 Ol	14/2 Plag	15/1 Plag	15/2 Plag	15/3 Aug	15/4 Aug	15/5 Aug	15/6 Aug	15/7 Aug	15/8 Aug	15/9 Aug	15/10 Plg
SiO ₂	40.15	48.04	50.43	—	39.83	48.29	50.75	40.77	50.91	51.72	64.90	53.69	50.94	51.84	51.88	51.45	51.19	51.01	52.16
Al ₂ O ₃	—	32.26	30.65	28.15	—	32.52	30.42	—	30.02	30.10	22.03	1.59	2.48	2.28	2.56	1.98	0.95	1.85	0.80
Cr ₂ O ₃	—	—	—	34.96	—	—	—	—	—	—	—	0.23	—	—	—	—	—	—	—
FeO ^a	12.67	0.52	0.51	19.70	14.21	0.55	0.51	13.29	0.47	0.45	0.46	5.50	8.61	9.07	8.99	13.76	18.84	12.80	21.30
MnO	0.21	—	—	0.53	—	—	—	0.26	—	—	—	0.14	0.22	0.22	0.24	0.31	0.66	0.30	0.66
MgO	46.55	—	0.26	15.07	45.15	0.26	0.23	45.50	0.27	—	—	17.91	15.38	16.00	16.91	16.62	11.79	14.39	19.21
NiO	—	—	—	0.26	—	—	—	—	—	—	—	—	—	—	—	—	—	—	—
CaO	0.19	17.39	15.19	—	0.29	16.91	15.07	0.26	14.99	14.16	3.35	20.43	20.12	19.17	18.18	14.79	16.21	17.70	5.45
Na ₂ O	—	1.50	2.52	—	—	1.67	2.74	—	2.56	3.43	9.67	—	0.28	0.31	0.28	0.29	0.34	—	—
K ₂ O	—	—	—	—	—	—	—	—	—	—	0.25	—	—	—	—	—	—	—	—
TiO ₂	—	—	—	0.61	—	—	—	—	—	—	—	0.39	0.91	0.75	0.73	0.61	0.51	1.09	0.60
Total	99.77	99.71	99.56	99.28	99.48	100.20	99.72	100.08	99.22	99.86	100.66	99.88	98.94	99.64	99.77	99.81	100.49	99.14	100.18
Cation Proportions No. of oxygens	4	32	32	32	4	32	32	4	32	32	32	6	6	6	6	6	6	6	6
Si	0.999	8.853	9.243	—	1.000	8.847	9.286	1.012	9.350	9.428	11.395	1.960	1.912	1.927	1.920	1.928	1.961	1.932	1.959
Al	—	7.008	6.623	8.044	—	7.024	6.563	—	6.499	6.469	4.560	0.069	0.110	0.101	0.112	0.087	0.043	0.083	0.036
Cr	—	—	—	6.701	—	—	—	—	—	—	—	0.007	—	—	—	—	—	—	—
Fe	0.263	0.079	0.077	3.975	0.297	0.084	0.078	0.275	0.072	0.068	0.067	0.167	0.269	0.281	0.277	0.430	0.601	0.404	0.666
Mn	0.005	—	—	0.109	—	—	—	0.006	—	—	—	0.005	0.007	0.007	0.007	0.010	0.022	0.010	0.021
Mg	1.726	—	0.071	5.443	1.690	0.071	0.064	1.684	0.074	—	—	0.974	0.861	0.887	0.933	0.928	0.674	0.812	1.076
Ni	—	—	—	0.050	—	—	—	—	—	—	—	—	—	—	—	—	—	—	—
Ca	0.005	3.434	2.983	—	0.008	3.318	2.956	0.007	2.949	2.767	0.631	0.799	0.810	0.764	0.721	0.594	0.666	0.719	0.220
Na	—	0.535	0.896	—	—	0.595	0.972	—	0.913	1.214	3.290	—	0.021	0.023	0.021	0.021	0.026	—	—
K	—	—	—	—	—	—	—	—	—	—	0.056	—	—	—	—	—	—	—	—
Ti	—	—	—	0.112	—	—	—	—	—	—	—	0.011	0.026	0.021	0.021	0.018	0.015	0.032	0.017
Σ	2.998	19.909	19.893	24.434	2.995	19.939	19.919	2.984	19.857	19.946	19.999	3.992	4.016	4.011	4.012	4.016	4.008	3.992	3.995

coprecipitation of plagioclase and clinopyroxene. In contrast, both the East Pacific Rise and OCP Ridge porphyritic lavas contain evidence in their phenocrysts of a rather complex crystallization history.

The evidence detailed in this chapter shows that calcic plagioclase precipitated before most, or even all, the other phenocrysts in these lavas. It is the sole phenocryst phase in Samples 421-3-1 (Piece 8) and 429A-2-1 (Piece 16) and occurs as cores within more-sodic plagioclase in six of the remaining 10 rocks studied, including at least one from each hole. In Sample 422-9-2 (Piece 4c), there is no doubt that a small amount of Cr-Al spinel coprecipitated with the calcic plagioclase. It is probable that clinopyroxene accompanied the liquidus plagioclase in the magmas of Samples 420-13, CC-1 and 423-8-1 (Piece 4). Nevertheless, the textural relationships between these minerals do not prove their coprecipitation beyond doubt. Calcic plagioclase is observed alone as the earliest phase in the remaining five occurrences in this study. The amounts are so small (Table 1) that another coprecipitated phase could easily fail to be represented in a pair of thin sections. Nevertheless, the absence of such phases—notably forsteritic olivine—from the entire available collection is probably significant. It should be noted that no inclusions of glass have been observed within the calcic plagioclases in any of the Leg 54 samples studied by the authors.

The interpretation of the crystallization history of phenocrysts in the Leg 54 lavas from the East Pacific Rise and OCP Ridge hinges on a decision whether the early-formed calcic plagioclases are xenocrysts (signifying magma mixing) or phenocrysts (subsequently thrown out of equilibrium with the magma by changing physical conditions). These alternatives have been debated by various authors in relation to most suites of ocean-floor lavas subjected to detailed study. In examples where a strong case has been made for magma mixing (e.g., Muir and Tilley, 1964, 1966; Donaldson and Brown, 1977; Dungan and Rhodes, 1978) some, at least, of the

large crystals in the rocks are blatantly xenocrystal. Their characteristic features are: large size (>1 mm); rounded or irregularly embayed shapes (with or without zoned overgrowths); random compositional relationships to those of euhedral microphenocrysts or skeletal glomerocrysts in the host lava (the megacrysts are either more or less refractory, or both); and abundant content of glass inclusions that are dissimilar in composition from the glass phase of the host lava. These inclusions are reported either in zones along crystal-growth planes or, most significantly, in irregular networks throughout crystals, suggesting the infilling of corrosion channels. Apart from rounding in some (but not all) instances, the Leg 54 East Pacific Rise and OCP Ridge calcic plagioclases show none of the listed criteria for xenocrysts. Therefore the mineralogical and textural evidence for magma mixing, in these particular ocean-floor lavas, is weak.

The data summarized in Table 2 show that the compositions of the calcic plagioclase phenocryst cores in Leg 54 lavas from the East Pacific Rise and OCP Ridge are systematically related to those of the phenocrysts enclosing them. Thus, the latter range from An₆₇ to An₇₇, while their cores range from An₇₉ to An₈₇. This feature may be reconciled with a magma-mixing genetic scheme by the introduction of ad hoc postulates. For instance, it may be supposed that the ratio of more primitive to more evolved melt in the mixture was high, so that the composition of the latter was "swamped" by the former in the final mixture. If this was the case, it is hard to see why the compositional gap between the calcic cores and surrounding phenocrystal plagioclase (9 to 12% An) is as large (and larger) as that between calcic xenocrysts and associated equilibrium plagioclase phenocrysts in published examples of mixed-magma lavas (e.g., Donaldson and Brown, 1977; Dungan and Rhodes, 1978).

In view of these features, it seems logical to consider the possibility that the calcic bytownite occurring as the

TABLE 3 — Continued

Sample Analysis No. Mineral	428A-6-1 (Piece 6)			427-10-3 (Piece 3)				427-11-1 (Piece 3)	
	16/1 Ol	16/2 Plag	16/3 Aug	17/1 Plag	17/2 Aug	17/3 Aug	17/4 Aug	18/1 Plag	18/2 Aug
SiO ₂	39.62	50.57	52.02	52.79	52.96	51.83	51.42	50.48	52.49
Al ₂ O ₃	—	30.24	2.82	29.73	1.96	3.30	1.21	30.30	2.81
Cr ₂ O ₃	—	—	1.14	—	0.40	0.42	—	—	0.62
FeO ^a	15.94	0.39	4.77	0.51	6.94	8.04	17.89	0.39	5.80
MnO	0.22	—	—	—	—	0.22	0.60	—	—
MgO	43.82	0.21	16.64	—	16.99	16.15	12.19	0.27	16.91
NiO	0.19	—	—	—	—	—	—	—	—
CaO	0.27	14.74	21.61	13.99	20.41	19.20	16.71	14.92	20.60
Na ₂ O	—	2.92	—	3.41	—	—	—	3.02	0.32
K ₂ O	—	—	—	—	—	—	—	—	—
TiO ₂	—	—	0.43	—	0.44	0.75	0.66	—	0.44
Total	100.06	99.07	99.43	100.43	100.10	99.91	100.68	99.38	99.99
Cation Proportions									
No. of oxygens	4	32	6	32	6	6	6	32	6
Si	0.999	9.307	1.915	9.550	1.943	1.911	1.956	9.274	1.923
Al	—	6.561	0.123	6.341	0.085	0.144	0.055	6.562	0.122
Cr	—	—	0.034	—	0.012	0.013	—	—	0.018
Fe	0.335	0.060	0.147	0.077	0.212	0.247	0.567	0.060	0.177
Mn	0.005	—	—	—	—	0.007	0.020	—	—
Mg	1.646	0.058	0.913	—	0.929	0.888	0.691	0.074	0.923
Ni	0.004	—	—	—	—	—	—	—	—
Ca	0.007	2.906	0.853	2.713	0.802	0.759	0.682	2.938	0.809
Na	—	1.043	—	1.197	—	—	—	1.076	0.023
K	—	—	—	—	—	—	—	—	—
Ti	—	—	0.012	—	0.013	0.021	0.019	—	0.012
Σ	2.996	19.935	3.997	19.878	3.996	3.990	3.990	19.984	4.007

Note: 1/1 = skeletal glomerocryst; 1/2 = euhedral calcic core in glomerocryst; 1/3 = euhedral unzoned phenocryst; 1/4 = anhedral glomerocryst; 2/1 = skeletal phenocryst; 2/2 and 2/3 = euhedral phenocrysts; 3/1 = core of euhedral phenocryst; 3/2 = rim of euhedral phenocryst; 4/1 = euhedral phenocryst; 4/2 = rounded calcic area in core of phenocryst; 4/3 = core of euhedral phenocryst; 4/4, 4/5, and 4/6 = skeletal groundmass glomerocrysts; 5/1 = skeletal glomerocryst; 5/2, 5/3, and 6/1 = euhedral phenocrysts; 6/2 = skeletal glomerocryst; 6/3 and 6/4 = anhedral glomerocrysts; 7/1 = euhedral phenocryst; 7/2 = subhedral phenocryst; 8/1 and 8/2 = skeletal glomerocrysts; 9/1 = core of euhedral phenocryst; 9/2 = rim of euhedral phenocryst; 10/1 = small round intergrown crystal; 10/2 = core of intergrown lath; 10/3 and 10/4 = cores of intergrown equant crystals; 10/5 = rim of intergrown equant crystal; 11/1 = small round intergrown crystal; 11/2 = core of intergrown lath; 11/3 = core of intergrown equant crystal; 12/1 = euhedral glomerocryst; 12/2 = euhedral calcic core in phenocryst; 12/3 and 12/4 = euhedral phenocrysts; 13/1 = euhedral glomerocryst; 13/2 = oval calcic core in glomerocryst; 13/3 = skeletal outer part of previous crystal; 14/1 and 14/2 = euhedral glomerocryst; 15/1 = core of intergrown lath; 15/2 = skeletal interstitial lath; 15/3 = unzoned euhedral crystal core; 15/4 = (010) sector of crystal inner mantle; 15/5 = (110) sector of crystal inner mantle; 15/6 = (100) sector of crystal inner mantle; 15/7 and 15/8 = rims of intergrown anhedral crystals; 15/9 = rim of intergrown anhedral crystal adjacent to pigeonite outgrowth; 15/10 = epitaxial overgrowth adjacent to previous analysis; 16/1 = small round intergrown grain; 16/2 = core of intergrown lath; 16/3 = core of intergrown equant crystal; 17/1 and 17/2 = subhedral phenocrysts; 17/3 = core of intergrown equant groundmass crystal; 17/4 = rim of intergrown equant groundmass crystal; 18/1 and 18/2 = subhedral phenocrysts.

^aTotal Fe as FeO.

^b— = oxide below detection limit.

sole phenocrysts in Samples 421-3-1 (Piece 8) and 429A-2-1 (Piece 16) and as calcic cores within phenocrysts in other East Pacific Rise and OCP Ridge lavas is cognate to the rocks in which it is found. In such a model an explanation must be forthcoming for the abrupt cessation of plagioclase-dominated early crystal assemblages, together with variable resorption (in most but not all cases) of the calcic bytownite. Both load pressure and p_{H_2O} affect the precipitation of plagioclase from basalt magma. If the plagioclase phenocryst cores in these lavas formed under high load pressures, they would be more sodic than the feldspar surrounding them—the opposite relationship from that observed. High p_{H_2O} causes the plagioclase precipitating from basalt magma to be more calcic than that which forms under anhydrous conditions.

Published studies of the volatiles contents of ocean-floor lavas from several localities demonstrate that, after their eruption and quenching, these rocks show few signs of ever having been hydrous magmas. Thus, Moore et al. (1977) have found that carbon dioxide comprises more than 95 per cent by volume of the gases filling vesicles within glassy pillow margins of several Atlantic and Pacific ocean-floor basalts. Delaney et al. (1978) and Muenow et al. (1979) have found CO₂-dominated vapor phases in the glass inclusions within olivine

and plagioclase phenocrysts and megacrysts (0.5 to 10 mm) in ocean-floor basalts from several localities. These authors have also shown that low water contents in phenocryst inclusions is not a worldwide feature of ocean-floor lavas; the crystal-enclosed glasses of basalts from the Marianas Interarc Basin have a high H₂O/CO₂ ratio. The pillow-margin glasses of all ocean-floor lavas studied by these authors show a high H₂O/CO₂ ratio. The carbon dioxide contents in these lavas appear to be sufficient to saturate the magmas at the pressures imposed by ocean depth at their extrusion sites, whereas the water contents seem to be below theoretical saturation values (except for the Marianas samples).

The data on volatiles appear to place substantial constraints upon any hypothesis postulating hydrous magmas beneath mid-ocean ridges. Nevertheless, when some of the apparent constraints are examined in detail, they are not so restrictive as they seem. For instance, when the H₂O/CO₂ ratios of glass inclusions within phenocrysts are used to deduce magmatic volatiles contents, it is assumed that these gases are trapped within the growing crystals in the same ratio as they occurred in the surrounding liquid. This may not be the case for water and carbon dioxide, as Delaney et al. (1978) clearly recognized. The glass inclusions studied by these investigators ranged from <1 μm to 1 mm in diameter (*op. cit.*, p.

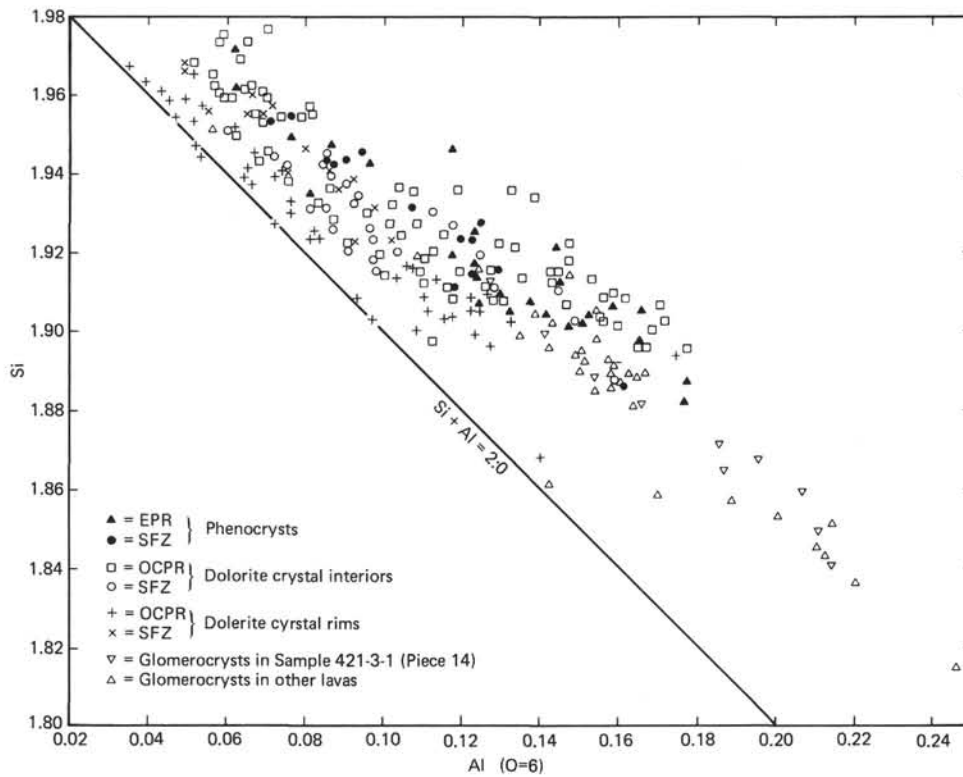


Figure 2. *Si versus Al (cation proportions on a 6-oxygen basis) in pyroxenes within basalts and dolerites from the East Pacific Rise (EPR), OCP Ridge (OCPR), and Siqueiros fracture zone. The key to the symbols is on the diagram.*

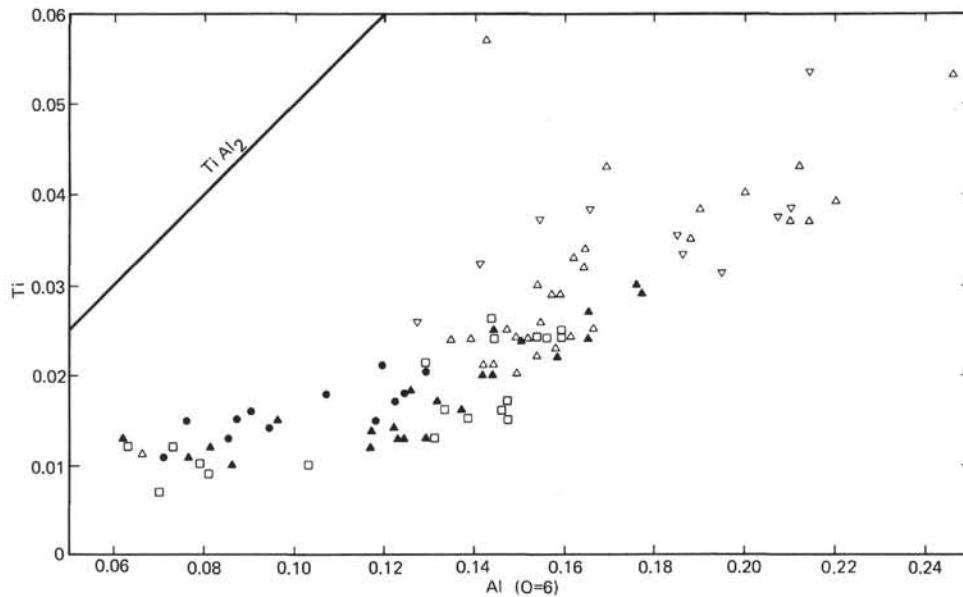


Figure 3. *Ti versus Al in the pyroxenes plotted on Figure 2, with the exception of the three dolerites studied in detail (see Figure 4). Symbols as in Figure 2.*

584). All but the smallest of these could be trapped by the growing face of a crystal only if this was forming so fast that skeletal protrusions surrounded small volumes of the adjacent liquid. Cellular outgrowth of the faces of a free-floating crystal requires a diffusion-controlled mechanism (Cahn, 1967). Local crystal-melt interface

instabilities arise through failure of crystal-forming components to diffuse fast enough through the liquid boundary layer, adjacent to the interface, to provide a uniform flux to the growing face. The diffusion coefficients at liquidus in basaltic melt of the various cations essential to the formation of olivine and calcic plagi-

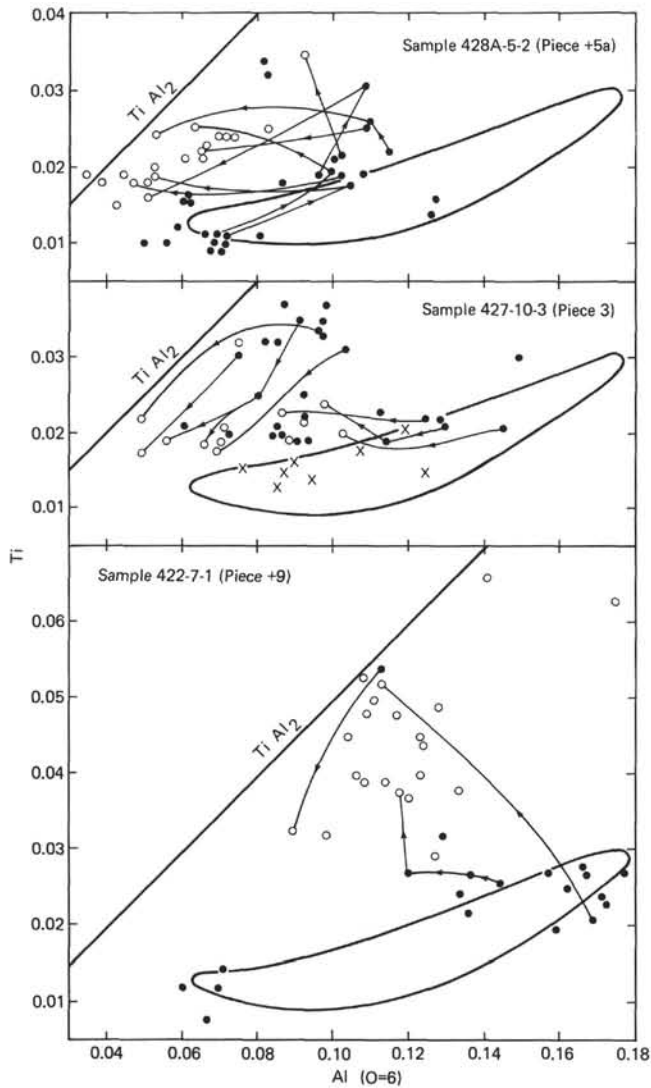


Figure 4. *Ti versus Al in pyroxenes within the three dolerites studied in detail. Key to symbols: X = phenocrysts in Sample 427-10-3(Piece 3); ● = interiors of crystals; O = rims of crystals. The fine arrowed lines are explained in the legend to Figure 6. The area enclosed with a bold line is the field occupied by analyses of pyroxene phenocrysts in porphyritic samples plotted on Figure 3.*

class range from about 3×10^{-6} to 10^{-7} cm²/s (Hofmann and Magaritz, 1977; personal communication, R. Lowry, 1979). The diffusion coefficient of carbon dioxide under similar conditions is 4×10^{-8} cm²/s (Muehlenbachs and Kushiro, 1974), whereas the coefficient for water is only about 2×10^{-5} cm²/s (Sparks, 1978). If the relative magnitudes of these diffusion coefficients are correct, it would seem possible that carbon dioxide may be retained strongly, relative to water, during the entrapment of glass within the phenocrysts of ocean-floor basalts.

Although it is generally assumed that the phenocrysts in ocean-floor lavas grew within some sort of magma chamber in the crust beneath spreading axes, there is lit-

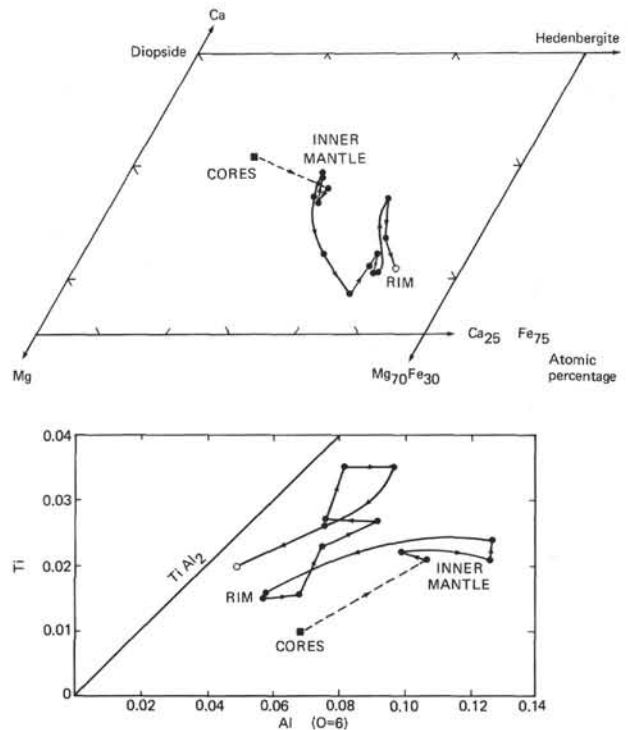


Figure 5. *Chemical zoning along a microprobe traverse across a single pyroxene crystal in OCP Ridge dolerite Sample 428A-5-2(Piece 5a). The spacing of the analyses is 40 microns, except for the three innermost points (150 μm). The symbols and fine arrowed lines are explained in the legends of Figures 4 and 6. In addition: ■ = average analysis of euhedral unzoned cores in pyroxenes of Sample 428A-5-2(Piece 5a).*

TABLE 4
Phase Appearance Sequence during Early Stages of Crystallization of Leg 54 Porphyritic Lava Samples

Sample	Liquidus Phases	Sub-liquidus phenocryst phases
420-13, CC (Piece 1)	Plag (An79) + Cpx	Glomerophytic Plag (An7) + Cpx
420-16-1 (Piece 1)	Ol + Plag + Cpx	Same phases in glomerocrysts
421-3-1 (Piece 8)	Plag (An3)	
421-3-1 (Piece 14)	Plag (An79)	Plag (An71) + Ol
421-4-1 (Piece 3)	Ol + Plag + Cpx (all glomerophytic)	
423-7-1 (Piece 6)	Plag (An71)	Glomerophytic Plag (An64) + Cpx
423-8-1 (Piece 4)	Plag (An72) + Cpx	Same phases in glomerocrysts
429A-2-1 (Piece 4a)	Ol + Plag (all glomerophytic)	
429A-2-1 (Piece 16)	Plag (An2)	
422-9-2 (Piece 4c)	Plag (An7) + Spinel	Glomerophytic Plag (An77) + Ol + Cpx
428-5-4 (Piece 2)	Plag (An5)	Glomerophytic Plag (An75) + Ol
428-6-2 (Piece 12)	Ol + Plag (all glomerophytic)	
427-10-3 (Piece 3)	Plag + Cpx	
427-11-1 (Piece 3)	Plag + Cpx	

tle positive evidence as to the depth of their formation. Thus, mixing models which postulate the ingress of phenocryst-laden primitive magmas into crustal reservoirs imply that their phenocrysts formed at greater depth, within the upper mantle. Bender et al. (1978) have proposed, on the basis of melting experiments, that the Ca-rich clinopyroxene occurring as sparse rounded and embayed "xenocrysts" in many ocean-floor lavas was initially precipitated at a depth of 30 km or more. Sigurdsson and Schilling (1976) have suggested that the Al-rich spinels found in some Mid-Atlantic Ridge lavas also crystallized at high pressures. It seems possible, there-

fore, that the comparatively large olivines and plagioclases analyzed for carbon dioxide and water by Delaney et al. (1978) and Muenow et al. (1979) were precipitated, while the magmas containing them were still within the upper mantle. Delaney et al. (1978) postulated influx of water into ocean-floor magmas rising beneath spreading centers, in order to explain the high H_2O/CO_2 ratio of their pillow-margin glasses. In view of the points discussed here, it seems logical to suggest that water entered these magmas while they were within the oceanic crust.

Edmond et al. (1979) have argued that, immediately beneath spreading axes, sea water penetrates the ocean crust to a depth of 3.2 to 4.2 km. There are many published petrological descriptions of dredged or drilled samples of unlayered gabbros—some enclosing dykes—which appear to have originated from the upper part of Layer 3 of the oceanic crust. The descriptions of hydrous minerals in these rocks (e.g., Cann, 1971; Christensen and Salisbury, 1975) show that they were exposed to abundant water at sub-solidus temperatures, and that some of it entered the magmas. Muenow et al. (1979) discussed how sea water might be incorporated into magmas below spreading centers, in the light of the various known isotopic parameters of these aqueous and silicate liquids. They suggested that, rather than entering the basic melt directly, most of the water was first incorporated into hydrous minerals in metabasites and then released into subsequent upwelling magma batches during contact metamorphism and dehydration of the hydroxylated phases.

The influx of only a small amount of water into an anhydrous basaltic magma—less than the amount necessary to saturate it at even low pressures—will cause a substantial reduction in the temperature of crystallization of plagioclase in the cooling liquid, relative to other silicates (Kushiro and Thompson, 1972), together with a shift of the composition of the precipitating feldspar toward anorthite. Using the data of Yoder (1969) (his fig. 4), it may be estimated that a p_{H_2O} of approximately 100 bars, or slightly less, would cause the precipitation of the calcic plagioclase phenocryst cores in these lavas. Such a p_{H_2O} value could be attained in magma within the upper part of Layer 3 of the oceanic crust by water as a minor component in a CO_2 -dominated dissolved vapor phase, as implied by the data of Delaney et al. (1978). The presence of mixed volatiles would prevent the application of results from simple hydrous systems (Yoder, 1969) to quantification of the relationship between p_{H_2O} and the composition of the crystallizing plagioclase. But the authors are unaware of any more appropriate data.

If the phenocryst textures in Leg 54 basalts are ascribed to a change in the physical conditions affecting the magmas, this change must be able to account for the following features: (1) abrupt cessation of growth of the calcic plagioclase phenocrysts, (2) resorption and reprecipitation or discontinuous normal zoning, giving in each case a jump of about 10 per cent An in the composition of the crystallizing plagioclase (Table 2). The

resorption of the calcic plagioclase is extreme in Samples 421-3-1 (Piece 14) and 428-5-4 (Piece 12). It may of course have gone to completion in other Leg 54 lavas.

A fall in p_{H_2O} during the uprise of the magmas from the top of Layer 3 to the ocean floor would explain the observed sequences of plagioclase phenocryst crystallization. Such a water loss from an upwelling magma would cause it to become supersaturated, allowing the rapid crystallization of the skeletal glomerophytic assemblages. Expansion of the plagioclase stability field, relative to that of ferromagnesian silicate phases, under these conditions (Kushiro and Thompson, 1972) would result in plagioclase-dominated glomerophytic clusters, as are observed particularly well in the eruptive unit from which Sample 422-9-2 (Piece 4c) (Plate 1) is taken.

The final upwelling of the magmas must have been comparatively rapid, in order to preserve the small calcic plagioclases from complete dissolution. This time restriction precludes the escape of their contained water by diffusion, which would in any case be an improbable postulate for water-undersaturated melts. We therefore posit that these crystal-poor, low-viscosity magmas vesiculated and lost part of their dissolved water very rapidly during effervescence within conduits between their magmas reservoirs and the ocean floor. The high surface-to-volume ratio implied for these conduits suggests that they were dykes.

At first sight, this postulate that water was lost during pre-eruption effervescence of the Leg 54 magmas contradicts the conclusions of Moore et al. (1977) and Delaney et al. (1978) that the gas species which becomes saturated and vesiculates in magmas upwelling beneath spreading axes is carbon dioxide. There is, in fact, no contradiction. As CO_2 bubbles nucleate, grow, and eventually escape from a magma containing a dissolved mixed-volatile phase, the undersaturated gases, such as water, will partition between the silicate liquid and the gas-filled bubbles, as discussed by Anderson (1975) and Mysen (1977). Paradoxically, therefore, the effervescence of CO_2 from a CO_2 -saturated magma would also reduce its water content. If the relatively high rates of bubble loss—suggested by Delaney et al. (1978)—are correct, the partitioning of water between bubbles and surrounding liquid may be controlled more by diffusion kinetics than equilibrium. It was noted above that water has a much larger diffusion coefficient than CO_2 in basalt magma. Efficient removal of water in escaping CO_2 bubbles therefore seems likely.

If this hypothesis is correct, the glomerophytic clusters are irrelevant to any discussion of phenocryst fractionation from the Leg 54 magmas within intratelluric reservoirs, because they precipitated in the near-surface dykes feeding the eruptions. The final stage of development of phenocryst textures in Leg 54 lavas was the local further post-extrusion growth of glomerocrysts, within the centers of pillows or thick flows.

The geophysical parameters of the East Pacific Rise in the area drilled during Leg 54 have been determined recently by Orcutt et al. (1975) and Rosendahl et al. (1976), and discussed by Rosendahl (1976). Humphris

and Thompson (accompanying chapter) give a general account of the postulated evolution of the Leg 54 magmas within the established geophysical constraints. One aspect of the overall model is relevant to this mineralogy chapter. Rosendahl (1976) argues that the seismic velocity distribution in the upper part of Layer 3 (1.5 to 3.5 km depth), beneath the axial horst of the East Pacific Rise, is such that calcic plagioclase must be the dominant mineral in the rocks at this depth. To quote him (*op. cit.*, p. 5310): "The rocks need not be true anorthosites but they may approach anorthositic gabbroic compositions. This is rather a startling conclusion in terms of existing models of oceanic crust." The present mineralogical studies of phenocrysts in East Pacific Rise lavas drilled during Leg 54, combined with the experimental data of Yoder (1969) concerning the anorthite content and high ratio of plagioclase to ferromagnesian minerals in the phases precipitating from hydrous basaltic magmas, lead to precisely the same "startling conclusion" as Rosendahl (1976).

Two further points need emphasis. First, the mineralogical record of the pre-quench evolution of the Leg 54 basalts, as contained in their phenocrysts, seems to extend only backwards to the stage where these magmas reached the uppermost part of Layer 3 in the EPR crust in a hydrous state. All inferences about the evolution of these magmas between their genesis and a level about 4 km or less beneath the surface must therefore be made entirely from the chemistry of the samples (Humphris and Thompson, accompanying chapter). Secondly, the record preserved in their phenocryst mineralogy shows that the OCP Ridge basalts passed through exactly the same near-surface stages of magmatic evolution as the East Pacific Rise samples. This observation carries obvious implications about the possible source of the OCP Ridge lavas which fall beyond the scope of this chapter.

CLINOPYROXENE CRYSTALLIZATION TRENDS IN THREE DOLERITES

Some of the OCP Ridge units drilled during Leg 54 were doleritic, with equigranular-interstitial and subophitic intergrowths of plagioclase and clinopyroxene, up to 3 mm in grain size. It is not completely clear whether these rocks come from sills or (probably) the interiors of thick lava flows. All the samples from Site 427 (Siqueiros fracture zone) are also dolerites, containing sparse plagioclase and augite phenocrysts (Plate 1, Figure 8). The pyroxene zoning in Samples 422-7-1 (Piece 9), 427-10-3 (Piece 3), and 428A-5-2 (Piece 5a), has been studied. Olivine ($Fe_{0.85}$) is present as small, sparse, rounded grains in Sample 422-7-1 (Piece 9). It also occurs, with similar textural relationships, in other OCP Ridge dolerites, such as Sample 428A-6-1 (Piece 6) (Table 2), but is absent from the two other samples studied in detail.

Pyroxene analyses from the three dolerites are summarized in Table 3 and Figures 2, 4, 5, and 6. The pyroxene crystals in all three samples have colorless cores

and pale brown rims, adjacent to interstitial areas rich in Fe-Ti oxide. Some grains show shadowy extinction, but virtually no definite sector-zoning can be detected optically.

Sample 422-7-1 (Piece 9)

On Figure 6 it is apparent that the centers of pyroxene grains in this sample show a wide range of Ca/Mg ratios at an approximately constant Mg/Fe ratio (from $Ca_{43}Mg_{46}Fe_{11}$ to $Ca_{31}Mg_{56}Fe_{13}$). Figure 4 shows that the Ti and Al contents of these grain-center analyses are strongly bimodal, at the extreme ends of the trend shown by East Pacific Rise and Siqueiros fracture zone pyroxene phenocrysts in Figure 3. It seems likely, therefore, that the varying core compositions in the Sample 422-7-1 (Piece 9) pyroxene grains are due to sector-zoning, with the Ca-Al-Ti-rich zone or zones forming the bulk of the crystals.

On Figure 6 the rims of the Sample 422-7-1 (Piece 9) pyroxenes show iron enrichment at constant Ca/Mg, relative to crystal cores. The extent of iron enrichment varies greatly from grain to grain at different points around the margin of each crystal. Figure 4 shows that the predominant Ti-Al trend from cores to rims of pyroxenes in this dolerite is for Ti to rise and Al to fall, so that the atomic ratio of these elements approaches $\frac{1}{2}$. It is apparent from Figure 2 that the amount of Al^{VI} in the pyroxenes of all three dolerites decreases from cores to rims of crystals. Chromium shows a similar trend, so that the only significant minor-element substitution in the rim pyroxene is $CaTiAl_2O_6$.

Sample 427-10-3 (Piece 3)

The pyroxene phenocrysts in this sample are homogeneous ($Ca_{41}Mg_{48}Fe_{11}$) in their major-element composition. Figure 6 shows that analyses of the cores of groundmass crystals include a group at $Ca_{40}Mg_{46}Fe_{14}$, plus scattered points within the same field as the zoning of individual grains. This is approximately toward ferrosilite, with concomitant rising Fe/Mg and falling Ca/Mg ratio. The trends of zoning within individual grains are irregular on Figure 6. In Figure 4 it is apparent that the main trend of Ti and Al variation is a decrease of both these elements from the cores to the rims of crystals. While the zoning of Al is the same in this sample as in Sample 422-7-1 (Piece 9), that of Ti is the opposite. It is tempting to attribute this relationship to the early precipitation of Fe-Ti oxide in Sample 427-10-3 (Piece 3). Consideration of Sample 428A-5-2 (Piece 5a), however, shows that the controlling factor is the fall in Ca/Mg ratio from cores to rims of crystals. Ca-poor pyroxene can incorporate much less Ti and Al than Ca-rich pyroxene.

Sample 428-5-2 (Piece 5a)

This was the coarsest of the three dolerites studied and proved to be the most satisfactory for detailed investigation (Plate 1, Figure 9). The texture of this sample is not strictly a homogeneous dolerite. Most of the rock consists of a coarse intergrowth of plagioclase and

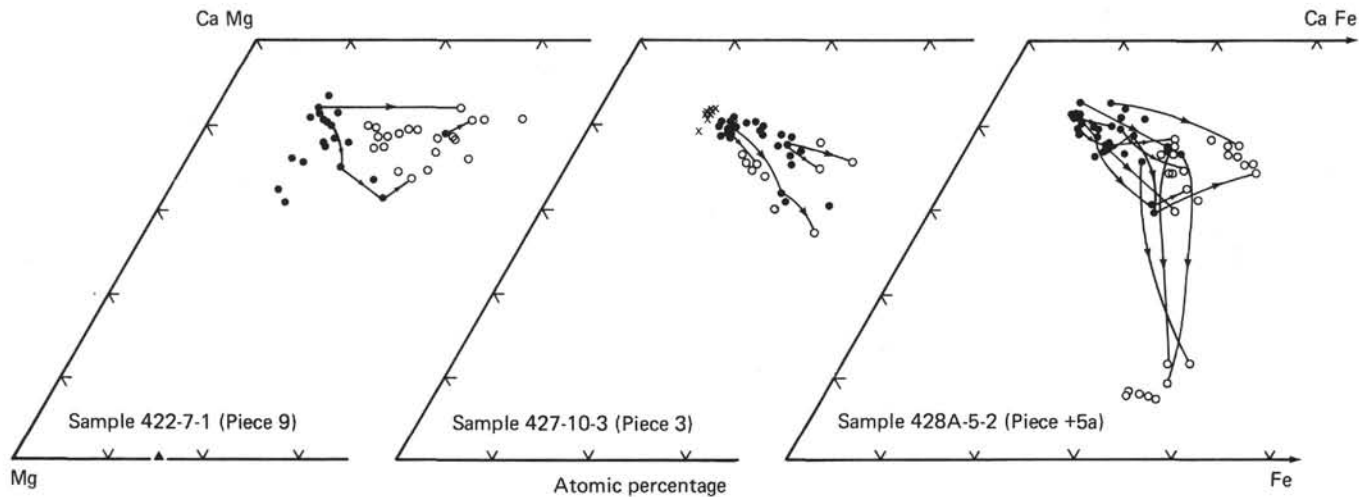


Figure 6. Atomic proportions of Ca, Mg, and Fe in the pyroxenes of three dolerites studied in detail. All Fe in each analysis is plotted, as consideration of charge balance suggests that little Fe^{+3} is present in most of these pyroxenes. The fine lines are not conventional tie-lines between coexisting phases: they join consecutive analyses on zoned grains, with the arrows pointing from cores to rims of crystals.

pyroxene, but there are also areas (a few per cent) of fine-grained skeletal plagioclase, pyroxene and Fe-Ti oxides.

When viewed through crossed nicols at extinction, some of the pyroxene crystals may be seen to have perfectly euhedral cores, showing sharp extinction (Plate 1, Figure 9). These are surrounded by mantles of pyroxene with shadowy extinction. The latter usually takes the form of progressive radial changes of a few degrees in extinction angle; only in one or two cases can very faint signs of optical sector-zoning be observed. The birefringence rises steadily in the outer mantles of these pyroxenes, toward their rims; this phenomenon is only prominent when it includes the first-order sensitive tint. The extent of marginal birefringence-zoning varies from point to point around the perimeter of each crystal, but is always greatest adjacent to a groundmass area. In some places there is local irregular banding, on a scale of 10 to 20 microns, of slight birefringence changes within the marginal high-birefringence zones. In contrast with the zoned pyroxenes in many alkalic rocks (e.g., Thompson, 1972), there is no sign in plane-polarized light of any fine-scale color banding within the Sample 428A-5-2 (Piece 5a) pyroxenes.

Textural relationships imply that the large zoned pyroxenes were coprecipitated with plagioclase alone. The euhedral pyroxene cores are mostly free from inclusions, but a few enclose plagioclase. The zoned mantles of the pyroxenes extend poikilitically around abundant plagioclases, while Fe-Ti oxides are confined to interstitial areas.

Microprobe analyses of the euhedral pyroxene crystal cores cluster around $Ca_{41}Mg_{50}Fe_9$ (Figure 6), with a Ca/Mg ratio range of 4 per cent Wo , which slightly exceeds analytical error. The inner parts of the zoned mantles surrounding the euhedral cores show a signifi-

cant range of Ca/Mg at approximately constant Mg/Fe ratio ($Ca_{42}Mg_{44}Fe_{14}$ to $Ca_{36}Mg_{50}Fe_{14}$). The outer mantles and rims of these pyroxenes show variable zoning along a scattered trend toward the ferrosilite apex of Figure 6, together with optically continuous overgrowths of very small amounts of pigeonite.

The almost total lack of optical sector-zoning in the Sample 428A-5-2 (Piece 5a) pyroxenes makes the role of this phenomenon in their chemical variation hard to study. Some progress has been made by focusing attention on the few sections which intersect the euhedral cores of the crystals, together with other diagnostic features such as cleavage and twinning. Use of such sections confirms that the inner mantles of these pyroxenes are Ca/Mg sector-zoned, with a high Ca/Mg ratio in the (110) and (010) sectors and low Ca/Mg ratio in the (100) sector (Table 3).

Analyses from the rims of crystals are very scattered on Figure 6. All the points on outer mantles and rims (from crystallographically indexed sectors) which plot near the sub-calcic augite field are in (100) sectors. Reconnaissance microprobe traverses across several crystals produce diverse zoning trends, including zigzags, on Figure 6. A single detailed traverse from core to rim of a crystal exhibiting strong marginal birefringence zoning is illustrated in Figure 5. It is not possible to index with certainty the crystallographic sector containing the traverse, because there is no euhedral core within this particular grain. Nevertheless, by analogy with other crystals, the sector appears to be (100). The rim of this crystal adjoins a groundmass area. While the overall Ca-Mg-Fe trend along this traverse is toward higher Fe/Mg ratio at the margin than in the core of the crystal, the most striking feature of Figure 5 is the strong oscillatory zoning of Ca/Mg, on a wavelength of about 300 microns, in the outer mantle of the grain. It is clear

that this radial oscillatory Ca/Mg zoning swamps the effects of any sector-zoning in the outer mantles and rims of these pyroxenes.

Ti-Al relationships in the Sample 428A-5-2 (Piece 5a) pyroxenes are complex (Figure 4). Analyses of euhedral crystal cores cluster around the point Ti = 0.01, Al = 0.07. Points on the inner mantles of grains have higher Ti (~0.02) and Al (~0.10) cation proportions but do not show any distinct sub-grouping of these elements, corresponding to sector-zoning. Points on the rims of crystals fall on the $TiAl_2$ line. The plot of Ti and Al along the detailed traverse (Figure 5) shows the complex way in which these two elements behave in the Sample 428A-5-2 (Piece 5a) pyroxenes. The remarkable zigzag, loop-the-loop course taken by this traverse reflects the control exerted upon the Ti and Al in this pyroxene by changes of Ca/Mg ratio during radial oscillatory zoning of the latter; a low Ca/Mg ratio correlates with low Ti and Al.

Pigeonite in Sample 428A-5-2 (Piece 5a)

Pigeonite is very rare in this sample. It occurs as tiny elongate epitaxial outgrowths from the rims of the large Ca-rich pyroxenes. These outgrowths never protrude into interstitial areas. In every case observed, one or both of the prism faces of the pigeonites (as seen in thin section) are in contact with plagioclase. The pyroxene of the main crystal immediately adjacent to each pigeonite overgrowth is not sub-calcic (Figure 6), but has a composition loosely clustering around $Ca_{36}Mg_{44}Fe_{20}$. The crystallographic sector of this outer-mantle pyroxene adjacent to pigeonite has been determined in one case; it is (110).

Discussion of Sample 428A-5-2 (Piece 5a) Pyroxenes

The zoning trends and pigeonite overgrowths exhibited by the pyroxenes in this sample are very similar to recorded features of pyroxenes in lunar basalts (Bence et al., 1971; Boyd and Smith, 1971; Hollister et al., 1971). The main difference is that the low f_{O_2} in the near-surface lunar environment permits extreme iron enrichment at the rims of lunar pyroxenes. The radial Ca/Mg zoning and appearance of marginal pigeonite in Sample 428A-5-2 (Piece 5a) show the same crystallographic control as in lunar lavas. Thus, Boyd and Smith (1971) (their figs. 1 and 2) have contrasted zoning within the (110) and (100) sectors of pyroxene phenocrysts in the lunar sample 12021. The (110) sector in 12021 pyroxene shows, within its inner mantle, an outward zoning trend of rising Fe/Mg ratio at constant Ca/Mg ratio (~ Wo_{35} , but with small Ca/Mg oscillations), followed by epitaxial pigeonite overgrowth. The inner mantle of the (100) sector in 12021 pyroxene has lower Ca/Mg (~ Wo_{28}) than (110). The outward (100) zoning trend is toward sub-calcic augite, with progressively higher Fe/Mg, and thence through gradual transition to pigeonite. Zoning in the (110) and (100) sectors of Sample 428A-5-2 (Piece 5a), described above, is extremely similar to that in the lunar pyroxenes reported by Boyd and Smith (1971), except that the sub-calcic trend in the

(100) sector is less pronounced in the terrestrial pyroxene.

Finally, some observations and inferences concerning the controls on pigeonite crystallization in Sample 428-5-2 (Piece 5a) are summarized. First, it is clear from Figure 6 that the relationship between Ca-rich and Ca-poor clinopyroxene in this dolerite is not that of an equilibrium solvus. This feature is consistent with the radial oscillatory and sector-zoning of the large augites, indicating metastable crystallization under supersaturated conditions. Secondly, pigeonite appears to have nucleated only upon the (110) faces of the large augites. Boyd and Smith (1971) present a full but inconclusive discussion of the possible factors that may cause the epitaxial overgrowth of pigeonite on some faces, such as (110), rather than others, such as (100), of augite. Thirdly, the pigeonite outgrowths appear to be excluded from groundmass areas and confined to sites in the rock where they have a prism face in contact with plagioclase. Such a textural relationship is, of course, difficult to demonstrate conclusively from the two-dimensional view afforded by a thin section. Nevertheless, it holds for every pigeonite crystal observed to date in this dolerite.

This pigeonite-plagioclase relationship may not be coincidental, but may result from nucleation of Ca-poor pyroxene occurring only on (or very near to) the surface of plagioclase crystals. The evidence given above for comparatively rapid metastable growth of the large zoned augites implies similar conditions for the coprecipitating, strongly zoned plagioclases in the rock. As these feldspars grew, the boundary layer of magma within a few microns of their advancing crystal faces would have been depleted in Ca and enriched in Mg and Fe, relative to the main body of interstitial liquid. Nucleation of Ca-poor pyroxene would be favored by the low Ca/(Mg+Fe) ratio in this boundary layer. Donaldson (1975b) has suggested a similar explanation for the occurrence of tiny inclusions, approximately sub-calcic augite in composition, arranged in concentric zones within the plagioclase phenocrysts of some basalt dykes. The combined pre-conditions of a (110) augite face touching a fast-growing plagioclase crystal, at the appropriate stage in the overall crystallization of the rock, would have been rare enough to explain the very sparse occurrence of pigeonite in Sample 428A-5-2 (Piece 5a).

ACKNOWLEDGMENTS

This study was possible only because of the unstinting efforts by P. Suddaby and N. Wilkinson to maintain the Imperial College microprobe system in peak operating condition. The Natural Environment Research Council provided the EDS detector, through Grant GR3/3357, and supports this work on ocean-floor rocks, through Grant GR3/2946. R. Lowry gave considerable assistance with discussion of diffusion in silicate liquids and access to unpublished data. The manuscript has benefited from the reviews and critical comments of I. L. Gibson, R. J. Kirkpatrick, M. A. Morrison, and J. H. Natland.

REFERENCES

- Anderson, A. T., 1975. Some basaltic and andesitic gases, *Rev. Geophys.*, v. 13, p. 37-57.
- Bence, A. E., Papike, J. J., and Ayuso, R. A., 1975. Petrology of submarine basalts from the central Caribbean: DSDP Leg 15, *J. Geophys. Res.*, v. 80, p. 4775-4804.
- Bence, A. E., Papike, J. J., and Lindsley, D. H., 1971. Crystallization histories of clinopyroxenes in two porphyritic rocks from Oceanus Procellarum. *Proceedings of the Second Lunar Science Conference: Cambridge (M. I. T. Press)*, v. 1, p. 559-574.
- Bender, J. F., Hodges, F. N., and Bence, A. E., 1978. Petrogenesis of basalts from the Project FAMOUS area: experimental study from 0 to 15 kbars, *Earth Planet. Sci. Lett.*, v. 41, p. 277-302.
- Boyd, F. R., and Smith, D., 1971. Compositional zoning in pyroxenes from lunar rock 12021, Oceanus Procellarum, *J. Petrol.*, v. 12, p. 439-464.
- Byerly, G. R., Melson, W. G., Nelen, J. A., and Jarosewich, E., 1977. Abyssal basaltic glasses as indicators of magma compositions, *Smithsonian Contrib. Earth Sci.*, No. 19, p. 22-30.
- Cahn, J. W., 1967. On the morphological stability of growing crystals. In Peiser, H. S. (Ed.), *Crystal Growth: Oxford (Pergamon Press)*.
- Cann, J. R., 1971. Petrology of basement rocks from Palmer Ridge, NE Atlantic, *Phil. Trans. Roy. Soc. Lond.*, v. A268, p. 605-617.
- Christensen, N. I., and Salisbury, M. H., 1975. Structure and constitution of the lower oceanic crust, *Rev. Geophys.*, v. 13, p. 57-86.
- Delaney, J. R., Muenow, D. W., and Graham, D. G., 1978. Abundance and distribution of water, carbon and sulfur in the glassy rims of submarine pillow basalts, *Geochim. Cosmochim. Acta*, v. 42, p. 581-594.
- Donaldson, C. H., 1975a. Calculated diffusion coefficients and the growth rate of olivine in a basalt magma, *Lithos*, v. 8, p. 163-174.
- , 1975b. Ultramafic inclusions in anorthite megacrysts from the Isle of Skye, *Earth Planet. Sci. Lett.*, v. 27, p. 251-256.
- , 1976. An experimental investigation of olivine morphology, *Contrib. Mineral. Petrol.*, v. 57, p. 187-213.
- Donaldson, C. H., and Brown, R. W., 1977. Refractory megacrysts and magnesium-rich melt inclusions within spinel in oceanic tholeiites: indicators of magma mixing and parental magma composition, *Earth Planet. Sci. Lett.*, v. 37, p. 81-89.
- Dungan, M. A., and Rhodes, J. M., 1978. Residual glasses and melt inclusions in basalts from DSDP Legs 45 and 46: evidence for magma mixing, *Contrib. Mineral. Petrol.*, v. 67, p. 417-431.
- Edmond, J. M., Corliss, J. B., and Gordon, L. I., in press. Ridge Crest—Hydrothermal metamorphism at the Galapagos spreading center and reverse weathering, *Ewings Symposium, Am. Geophys. Union*, v. 2.
- Hekinian, R., Moore, J. G., and Bryan, W. B., 1976. Volcanic rocks and processes of the Mid-Atlantic Ridge rift valley near 36° 49' N, *Contrib. Mineral. Petrol.*, v. 58, p. 83-110.
- Hofmann, A. W., and Magaritz, M., 1977. Equilibrium and mixing in a partially molten mantle. In Dick, H. J. B. (Ed.), *Magma Genesis: Bull. Oregon Dept. Geol. Mineral Ind.*, v. 96, p. 37-41.
- Hollister, L. S., Trzcinski, W. E., Jr., Hargraves, R. B., and Kulick, C. G., 1971. Petrogenetic significance of pyroxenes in two Apollo 12 samples. *Proceedings of the Second Lunar Science Conference: Cambridge (M. I. T. Press)*, v. 1, p. 529-557.
- Kushiro, I., and Thompson, R. N., 1972. Origin of some abyssal tholeiites from the Mid-Atlantic Ridge, *Carnegie Inst. Wash. Yearbook*, v. 71, p. 403-406.
- Lofgren, G. E., and Donaldson, C. H., 1975. Curved branching crystals and differentiation in comb-layered rocks, *Contrib. Mineral. Petrol.*, v. 49, p. 309-319.
- Moore, J. G., Batchelder, J. N., and Cunningham, C. G., 1977. CO₂-filled vesicles in mid-ocean basalt, *J. Volcanol. Geotherm. Res.*, v. 2, p. 309-327.
- Muehlenbachs, K., and Kushiro, I., 1974. Oxygen isotope exchange and equilibrium of silicates with CO₂ or H₂O, *Carnegie Inst. Wash. Yearbook*, v. 73, p. 232-236.
- Muenow, D. W., Graham, D. G., Liu, N. W. K., and Delaney, J. R., 1979. The abundance of volatiles in Hawaiian tholeiitic submarine basalts, *Earth Planet. Sci. Lett.*, v. 42, p. 71-76.
- Muir, I. D., and Tilley, C. E., 1964. Basalts from the northern part of the Rift Zone of the Mid-Atlantic Ridge, *J. Petrol.*, v. 5, p. 409-434.
- , 1966. Basalts from the northern part of the Mid-Atlantic Ridge. II. The *Atlantis* collections near 30°N, *ibid.*, v. 7, p. 193-201.
- Mysen, B. O., 1977. Solubility of volatiles in silicate melts under the pressure and temperature conditions of partial melting in the upper mantle. In Dick, H. J. B. (Ed.), *Magma genesis: Bull. Oregon Dept. Geol. Mineral Ind.*, v. 96, p. 1-14.
- Orcutt, J., Kennett, B., Dorman, L., and Prothero, W., 1975. Evidence for a low velocity zone underlying a fast-spreading rise crest, *Nature*, v. 256, p. 475.
- Roeder, P. L., and Emslie, R. F., 1970. Olivine-liquid equilibrium, *Contrib. Mineral. Petrol.*, v. 29, p. 275-289.
- Rosendahl, B. R., 1976. Evolution of oceanic crust, 2. Constraints, implications, and inferences, *J. Geophys. Res.*, v. 81, p. 5305-5314.
- Rosendahl, B. R., Raitt, R. W., Dorman, L. M., Bibee, L. D., Hussong, D. M., and Sutton, G. H., 1976. Evolution of oceanic crust, 1. A physical model of the East Pacific Rise crest derived from seismic refraction data, *ibid.*, v. 81, p. 5294-5304.
- Sigurdsson, H., 1977. Spinel in Leg 37 basalts and peridotites: phase chemistry and zoning. In Aumento, F., Melson, W. G., et al., *Initial Reports of the Deep Sea Drilling Project*, v. 37: Washington (U.S. Government Printing Office), p. 883-891.
- Sigurdsson, H., and Schilling, J.-G., 1976. Spinel in Mid-Atlantic Ridge basalts: chemistry and occurrence, *Earth Planet. Sci. Lett.*, v. 29, p. 7-20.
- Smith, D., and Lindsley, D. H., 1971. Stable and metastable augite crystallization trends in a single basalt flow, *Am. Min.*, v. 56, p. 225-233.
- Sparks, S. R. J., 1978. The dynamics of bubble formation and growth in magmas: a review and analysis, *J. Volcanol. Geotherm. Res.*, v. 3, p. 1-37.
- Thompson, R. N., 1972. Oscillatory and sector zoning in augite from a Vesuvian lava, *Carnegie Inst. Wash. Yearbook*, v. 71, p. 463-470.
- , 1974. Primary basalts and magma genesis. I. Skye, north-west Scotland, *Contrib. Mineral. Petrol.*, v. 45, p. 317-341.
- , in press. Major-element chemistry of basaltic glasses in Hole 418A lavas and a dyke: DSDP Legs 52 and 53. In Donnelly, T., Francheteau, J., Bryan, W., Robinson, P.,

Flower, M., Salisbury, M., et al., *Initial Reports of the Deep Sea Drilling Project*, v. 51, 52, 53: Washington (U.S. Government Printing Office).

Yoder, H. S., Jr., 1969. Calcalkaline andesites: experimental data bearing on the origin of their assumed characteristics. In McBirney, A. R. (Ed.), *Proceedings of the Andesite Conference: Oregon Dept. Geol. Mineral Ind. Bull.*, v. 65, p. 77-89.

PLATE 1

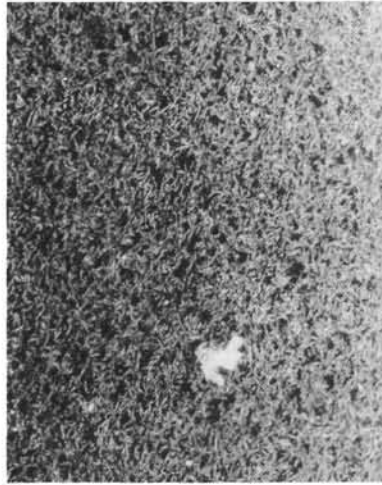
Length of scale bar is 1.5 mm.

- Figure 1 Phenocrysts of plagioclase and attached augite in a groundmass of glomerophyric clusters of these phases, within devitrified glass. Sample 423-8-1 (Piece 4).
- Figure 2 Phenocrysts of plagioclase and a single olivine in a groundmass of glomerophyric clusters of these phases. Note the slight flow alignment of the groundmass plagioclase. Sample 421-3-1(Piece 14).
- Figure 3 Glomerophyric clusters of plagioclase and olivine in fresh glass. Sample 429A-2-1(Piece 4a).
- Figure 4 Glomerophyric clusters of plagioclase and olivine in devitrified glass. Note the flow alignment of the plagioclase. Sample 428-6-2(Piece 12).
- Figure 5 Glomerophyric clusters of plagioclase and olivine in devitrified glass. Sample 428-5-4(Piece 2).
- Figure 6 Patchy texture, varying from near-aphanitic to glomerophyric. Microprobe studies allow the division of the plagioclase and augite crystal populations into liquidus phenocrysts and sub-liquidus glomerocrysts (see text). Sample 420-13,CC(Piece 1).
- Figure 7 Most of the crystals are plagioclase, olivine, and augite in abundant glomerophyric clusters. The largest of the calcic-bytownite liquidus phenocrysts in this section is visible at lower middle left. This crystal encloses a tiny euhedral Cr-Al spinel. Sample 422-9-2(Piece 4c).
- Figure 8 Phenocrysts of plagioclase and augite in a doleritic groundmass. Sample 427-10-3(Piece 3).
- Figure 9 Augite crystal within dolerite. Sample 428A-5-2 (Piece 5a). The section is cut approximately perpendicular to the z axis of this crystal. Note the euhedral core, zoned mantle and rims (intergrown with plagioclase), trace of {110} cleavage and development of a euhedral crystal outline adjacent to a (dark) groundmass area.

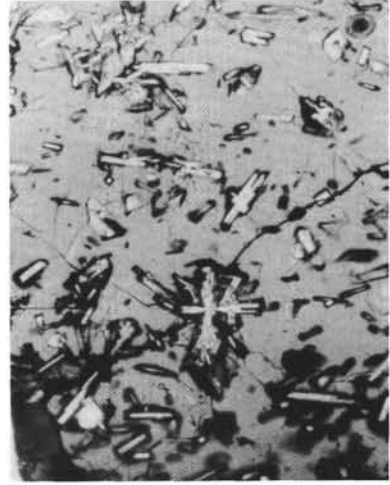
PLATE 1



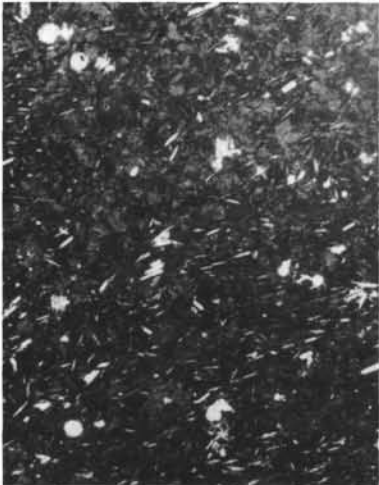
1



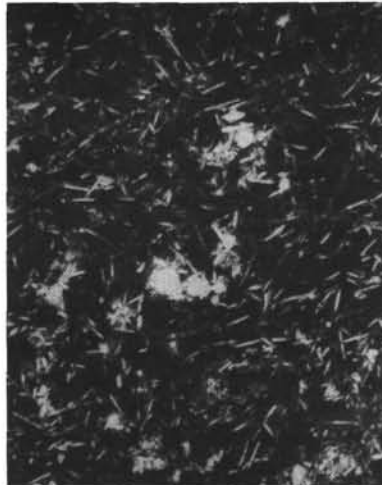
2



3



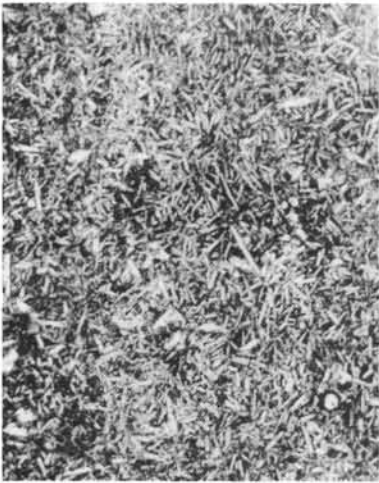
4



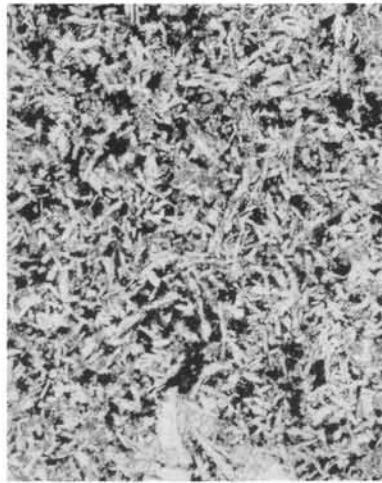
5



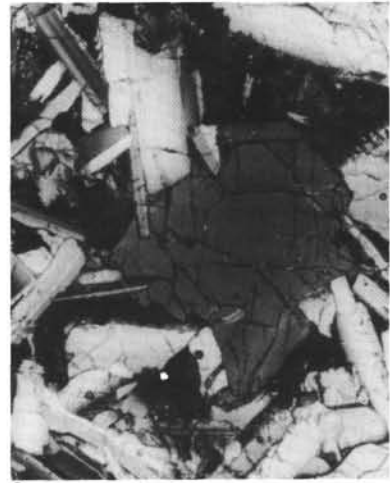
6



7



8



9